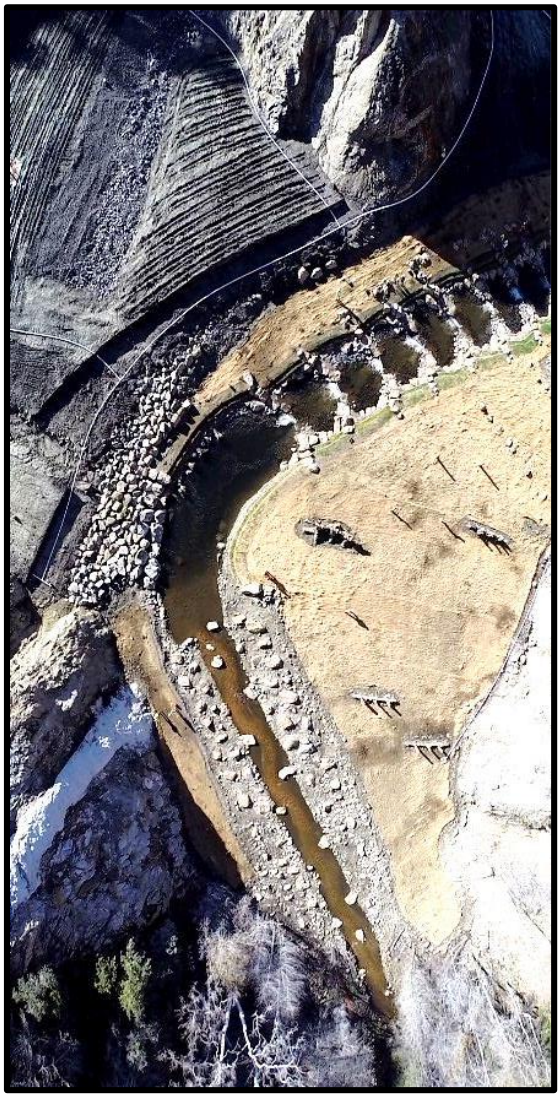

First Year Assessment of the Carmel River Reroute and Dam Removal Project

CSUMB Class: GEOL 460 Spring 2016

Laura Marson (Chief Editor)
Jordan Besson
California Biordi
Anna Conlen
Katrina DeWolf
Mitch Gravelle
Hannah Hubbard
Laura MacSween
Ronell Santos
Mia Sosa
Kelsey Thompson
Jocelyn Trejo-Arce
Douglas Smith, PhD (Instructor)

28 May 2016

Division of Science and Environmental Policy

California State University Monterey Bay

100 Campus Center, Seaside, CA, 93955

Acknowledgements

- This work was partially funded by UC Santa Cruz Fish Ecology Grant to Smith
- Granite Construction facilitated the study in several ways (David Hamblin, Michael Barnhart, Bill McGowan, Brian Hussar, Drew Archer, Elizabeth Geissler)
- Tetratech provided technical information (Bob Mussetter, Mike Brown)
- NOAA provided reference reach geomorophic data (Lee Harrison, Tommy Williams, David Boughton, Lea Bond, Colin Nicol)
- USGS provided reference reach geomorphic data (Amy East, Joshua Logan)
- Monterey Peninsula Management District (Greg James) provided stream flow data
- CSUMB Watershed Geology Lab provided technical field support (Kaitlyn Chow and Lauren Luna)
- Elsevier permitted us to reproduce figures from Chartrand et al. (2011)
- Wildland Hydrology (Kae Rosgen) gave permission to reproduce several figures from Wildland Hydrology publications
- Granite Construction allowed us to reproduce figures from design drawings (TetraTech (2012))
- AECOM (Steven McNeely) permitted us to reproduce the URS (2012) project basemap.
- California American Water Co. (Catherine Stedman) allowed us to use their post-construction drone photography in our assessment.
- Dr. Diana Lieberman and Kaitlyn Chow provided editorial comments.

This report was prepared for Granite Construction and the broad community involved in decommissioning San Clemente Dam. Kleinfelder Incorporated was the lead project designing firm. The channel design team was Tetra Tech Incorporated.

The report represents mentored undergraduate college student work completed within the constraints of a semester-long class.

The report may be cited as:

[GEOL 460] Marson L, Besson J, Biordi C, Conlen A, DeWolf K, Gravelle M, Hubbard H, MacSween L, Santos R, Sosa M, Thompson K, Trejo-Arce J, Smith D. 2016. First Year Assessment of the Carmel River Reroute and Dam Removal Project. Division of Science and Environmental Policy. Senior Thesis Report, 101 pp.

Executive Summary

The San Clemente Dam controlled the Carmel River from 1921 to 2015. In 2015, when the dam was removed, the reservoir sediment stockpile was stabilized with vegetation and a new channel and floodplain system was constructed to create easy migration for steelhead trout (anadromous *Oncorhynchus mykiss*), and to transport the annual flow of water, sediment, and wood past the old dam site.

Students in the River Hydrology and Monitoring (Geol 460) course at California State University of Monterey Bay conducted a reconnaissance-level study on the newly constructed channel following the first winter of operation. The results are based upon twelve students collecting data for two and a half days and analysis of design parameters supplied by Granite Construction. The primary goals of this study were to: 1) assess geomorphic adjustments that occurred during the first winter runoff following construction, 2) evaluate why any adjustments might have occurred and 3) establish a baseline for long term monitoring of the restoration project.

We found that most of the project performed as expected, with little change from post-construction conditions. However, the Upper Carmel River reach and some sections of the Combined Flow reach showed significant change. As of now, none of these physical changes appear severe enough to hinder fish passage. On the other hand, these adjustments to the project happened prematurely. The channel banks and crest nucleus boulders (CNBs) were designed to withstand a 25-year and 50-year flooding event, respectively. However, the peak flows that caused adjustments to the project thus far were less than the 1.5 year event (partial duration series).

Our main findings include the following points.

1) The river channel and floodplain were constructed as shown in the blueprints.
2) The CNBs may have moved prematurely because the density of sandstone used in the berm structures was 5% less than granite, which was used for

stability modeling in the design process. A 5% reduction in density yields a 7% reduction in estimated resistance to transport (critical shear).

3) Stability analysis used in the project design assumed the CNBs were spheres that would move only if forced to roll over a low fulcrum. The CNB shapes approximated rectangular solids that might slide rather than tip, so there is uncertainty in how well the stability analysis modeled the real system.
4) The constructed channel morphology was comparable to naturally stable river channels, except that pool-to-pool spacing might be low in the step-pool sections. Low pool spacing might also have influenced CNB stability.
5) The radius of curvature is locally smaller than stable reference streams. We found that the curves in the river that had tight bends experienced more erosion than those with larger values, as expected from the literature.
6) There is a relationship between channel slope and bank condition, with more bank adjustment occurring in reaches with higher slopes.
7) The down-valley floodplain gradient was locally steep enough to allow flood water to develop a nascent avulsion channel.

We surveyed six benchmarked cross-sections in the Reroute reach for long-term monitoring of the restoration project. We also performed pebble counts along our cross sections and on point-bars throughout the site, which showed that the river is successfully transporting the sediment that is being supplied to it.

The main goal of this restoration project was to ensure easy passage for the steelhead, so the restoration project can be considered a success following one year of winter flow. The removal of the San Clemente Dam has had far less downstream impacts than past dam removal projects and will be a good example to follow for future dam removal projects.

Table of Contents

1 Introduction

1.1 Project Overview

River restoration is becoming increasingly popular in the United States for a variety of reasons including to reduce erosion, improve water quality, and protect aquatic biodiversity (Bernhardt et al. 2007). However, post-restoration monitoring efforts are infrequent (Bernhardt et al. 2007). Post-restoration monitoring is not only important to ensure river restoration projects are actually successful in their goals, but also to contribute to the overall knowledge of successful river channel design (Endreny and Soulman 2011). Long-term post-restoration monitoring is needed to confidently identify best and worst practices in channel design. The purpose of this study is to monitor the stability of a newly constructed river channel through time in an effort to improve future river restoration design.

This study reviews the first-year performance of a new river and floodplain system constructed before winter runoff of the 2016 water year. The new river project is a key part of the decommissioning of San Clemente Dam. While this project is not "restoration" of an existing river, the design relies on many of the same methods and principles used in the river restoration industry.

1.2 Study Area

The Carmel River watershed drains approximately 247 square miles of land located at the northern end of the Santa Lucia Mountains of the California Coastal Ranges (Fig 1; U.S Geological Survey 2016). The study area for the Carmel River assessment is located at the former location of San Clemente Dam, about 18.5 miles upstream of the Pacific Ocean (Boughton et al. 2016). The drainage area above the study site is approximately 126 mi^2. Land use upstream of the study site consists of very minor residential and commercial use, but is mostly dominated by chaparral, grasslands, oak woodland, and conifer and redwood forests (Smith et al. 2004).

1.2.1 San Clemente Dam History

The San Clemente Dam (Fig. 1) was constructed in 1921 as a municipal water project to deliver water to the ever-growing Monterey population. The dam originally held an excess of 1,400 acre-feet of water, but was reduced to 70 acre-feet by 2008 (SDR 2016). The reason for this reduction of volume was primarily due to excess sediment build-up within the reservoir. In 1992, the California Department of Water Resources determined that the dam was not fit to withstand a large earthquake and could fail catastrophically if one were to occur. It was decided in 2008 that the dam would be removed and the river would be rerouted to accommodate steelhead migrations and spawning habitat.

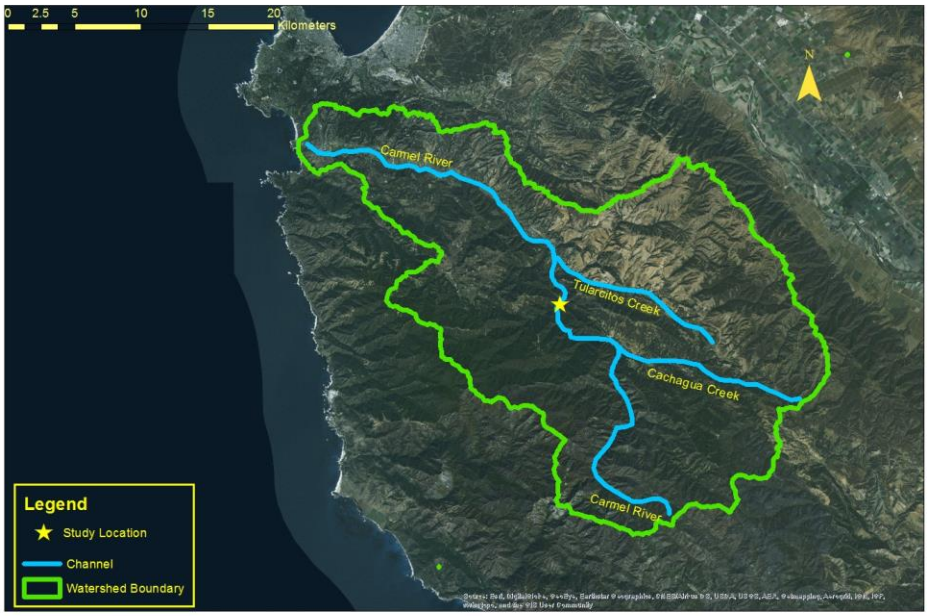

Figure 1. Location of project site within Carmel River Watershed. Double line indicates downstream limit of study site watershed.

The removal of the San Clemente dam is important because it is the largest dam to be removed in California, and the first dam removal that keeps the trapped sediment on site, rather than allowing a catastrophic sediment release.

1.2.2 Geology

In order to understand the Carmel watershed, we first need to understand the underlying geology. The geology of a watershed is one of the most important aspects of a watershed; it determines how erodible the ground is, if landslides will occur, and potential future land usage. The Carmel watershed is mainly on two mountain ranges, the Santa Lucia Range and the Sierra de Salinas Range (Smith et al. 2004). For the past two million years, these two mountain ranges have been uplifting at considerable rates (Smith et al. 2004). These uplifting events cause rivers to constantly cut down into the surrounding bedrock, which creates "V"-shaped valleys over time. The Santa Lucia Range is mainly composed of a small amount of sedimentary rocks from the Cenozoic era and granitic and metamorphic rocks from the pre-Cenozoic era (Rosenberg 2001). The Sierra de Salinas Range is composed of a weaker metamorphic rock that is called the "Schist of Salinas," granitic rock, and Tertiary sedimentary rocks which include Monterey Shale and sandstone (Smith et al. 2004).

The "V"-shaped valleys are more likely to occur in the Santa Lucia Range since it is made up of stronger bedrock material. The combination of the rock types in the Sierra de Salinas Range create the perfect condition for erosion and soil slips to occur, especially in the case of high slopes (Smith et al. 2004). This geology causes the rivers in the Carmel Watershed to have a very large amount of sediment supplied to them. The average annual load of sediment to the site is estimated to be 15 acre-ft, but can reach 90 acre-ft in extreme years (MEI 2003; MEI 2005). This high supply led to the premature filling of the San Clemente Dam Reservoir with sediment. The high sediment supply also poses a challenge for stream restoration designs, given that the system must effectively transport the sediment load to the lower Carmel River while maintaining its general shape.

1.2.3 Hydrology

The Carmel River watershed has a mild Mediterranean climate where the only source of water is through precipitation. The watershed receives 41 in/yr in the Santa Lucia Mountain Range and 14 in/yr at the mouth of the river. As storm events hit the Central Coast, the southwestern portion of the watershed sees

high rainfall amounts, leaving the northern parts of the Carmel River in a rain shadow with significantly less rainfall. The Carmel watershed has historically experienced droughts as well as major flooding events due to El Niño events (Smith et al. 2004).

Flood frequency for this study was calculated using discharge measurements from two stream gages located near Carmel River Reroute project (Fig. 2). The Sleepy Hollow gage was established by California American Water Company when the weir was created in 1988. It is located approximately one mile downstream of the reroute project. The drainage area of the Sleepy Hollow stream gage is 126 mi^2 (James 2009). The second stream gage, Robles del Rio, is located approximately three miles downstream from the project site (Fig. 2). The Robles del Rio gage has been managed by the USGS since 1957 (USGS). Robles Del Rio has a drainage area of 193 mi^2 and has a stage datum of 268.57 feet above sea level (NGVD29).

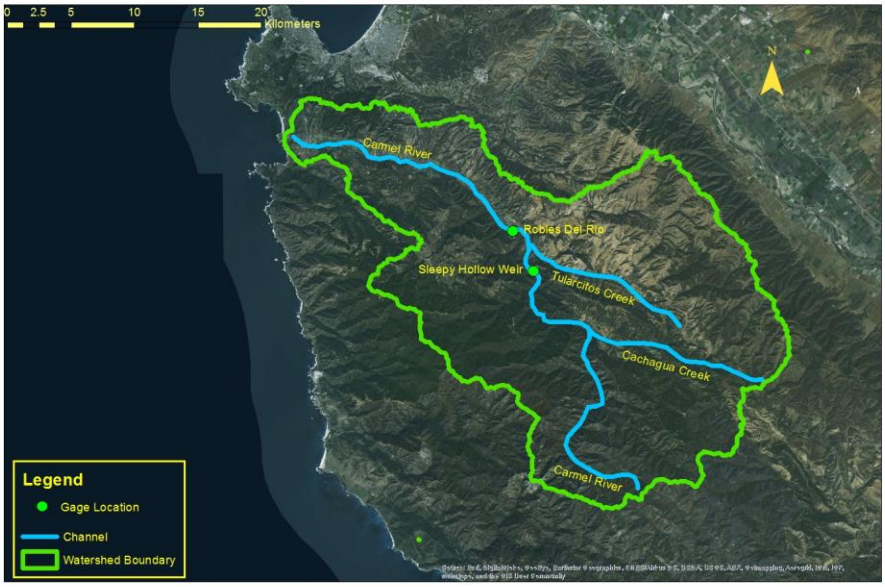

Figure 2. Location of Sleepy Hollow and Robles del Rio stream gages.

1.3 San Clemente Dam Removal and Carmel River Reroute

Recent large dam removal projects have included intentional catastrophic releases of sediment and have ended with the river flowing within its original channel. If the Carmel River were allowed to flow in its original course after the dam removal, the sediment that had collected in the reservoir would have been transported downstream, potentially causing massive flooding events and ecological impacts for federally listed species. Instead of relocating the 2.5 million cubic yards of reservoir-filling sediment to another location, which would not only have had great economic costs, but also environmental impacts, it was decided to reroute the Carmel River into the San Clemente Creek (Fig. 3). With this plan in place, the large sediment buildup remains in its original area; it was vegetated and assimilated into the natural surrounding landscape (SDR 2016). The Carmel River reroute and dam removal project (CRRDR) is the largest dam removal project that has occurred in California. This project could set a precedent for all future dam removal projects.

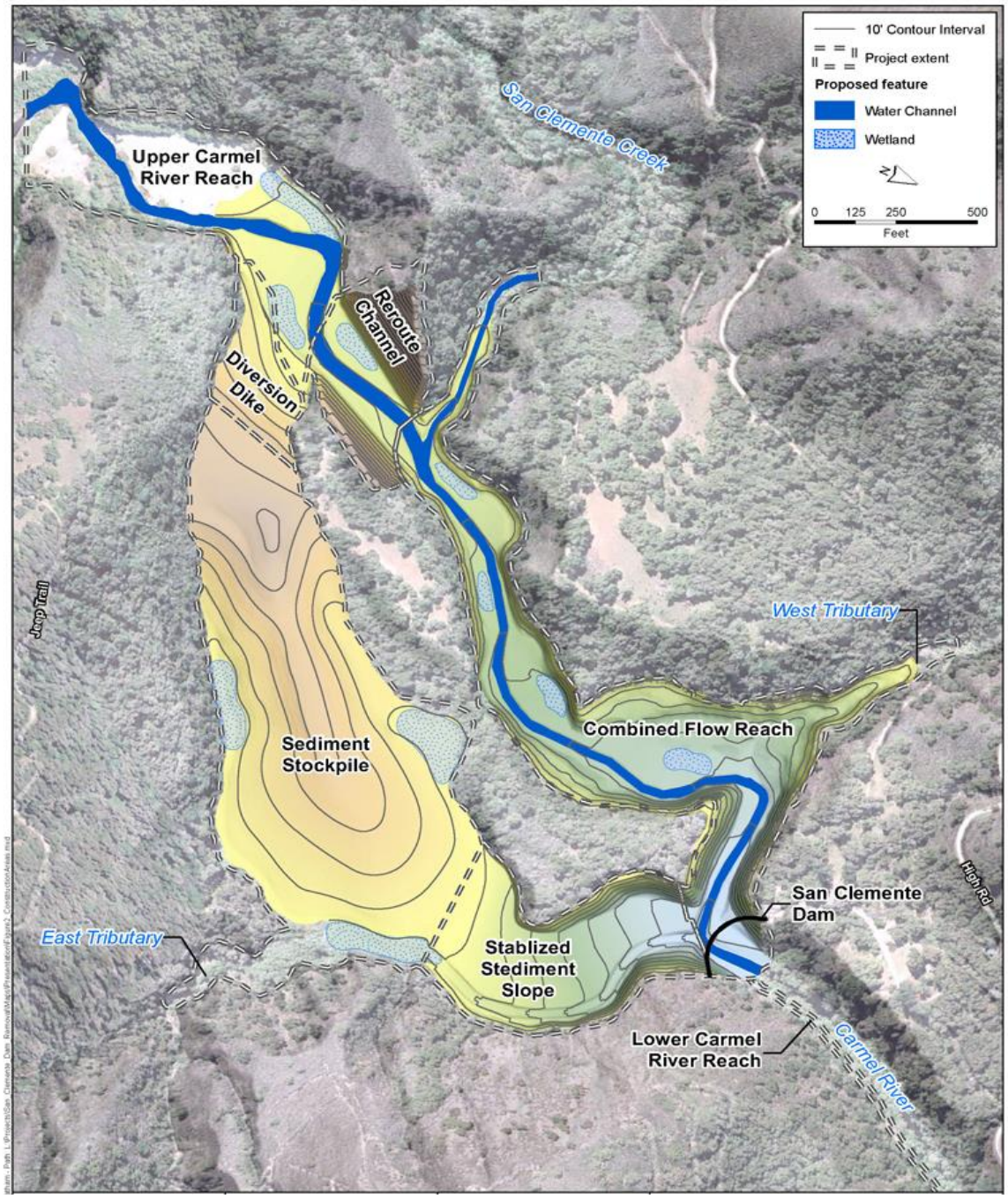

Figure 3. San Clemente Dam Removal and Carmel reroute project areas (URS 2012).

The rerouted channel was designed to reflect a natural stream channel that conforms to relevant fluvial geomorphic principles, while also providing unimpaired access to spawning habitat for steelhead. The goals for this project were set by Tetra Tech (2015):

1) The continuation of a sustainable fish passage that can adapt to changing flood conditions, with a focus on steelhead migration upstream and the migration of multiple species downstream,
2) The sustainability of the river channel itself in regards to river processes and functions,
3) The aquatic and riparian habitats that surround the site need to be of high quality and maintain fish passage,
4) The design of the river needs to meet natural variability and be consistent with the wildland setting of the Carmel River.

This project is a large scale experiment in river engineering that uses both time-honored fluvial geomorphic principles, emerging geomorphic ideas about step-pool geometry, and sediment transport theory. Natural river systems and hydraulic modeling were the main bases for channel design. For the step-pool sections of the river, the designs were based upon of natural forming step-pools that were found farther up the Carmel watershed (SDR 2016). However, the EDR (Environmental Data Resources) report put a one-foot maximum drop restriction between the step-pools to provide easier passage for the steelhead (Referenced in Tetra Tech 2015).

The total reach of the CRRDR project is about 4,125 feet long. The combined flow reach is approximately 2,500 feet long, the reroute reach is 625 feet long, and the upper Carmel River reach is about 1,000 feet long (Fig. 3; Tetra Tech, 2015). The combined flow reach contains a series of eight different stop-pool sections that range from 125 to 200 feet in length (Fig. 4). The reroute reach was designed to have riffle pool morphology, with two pools located at the bends in the constructed river channel (Tetra Tech, 2015). The upper Carmel River reach was included in the project to address the transition from the river outside of the site into the restoration site.

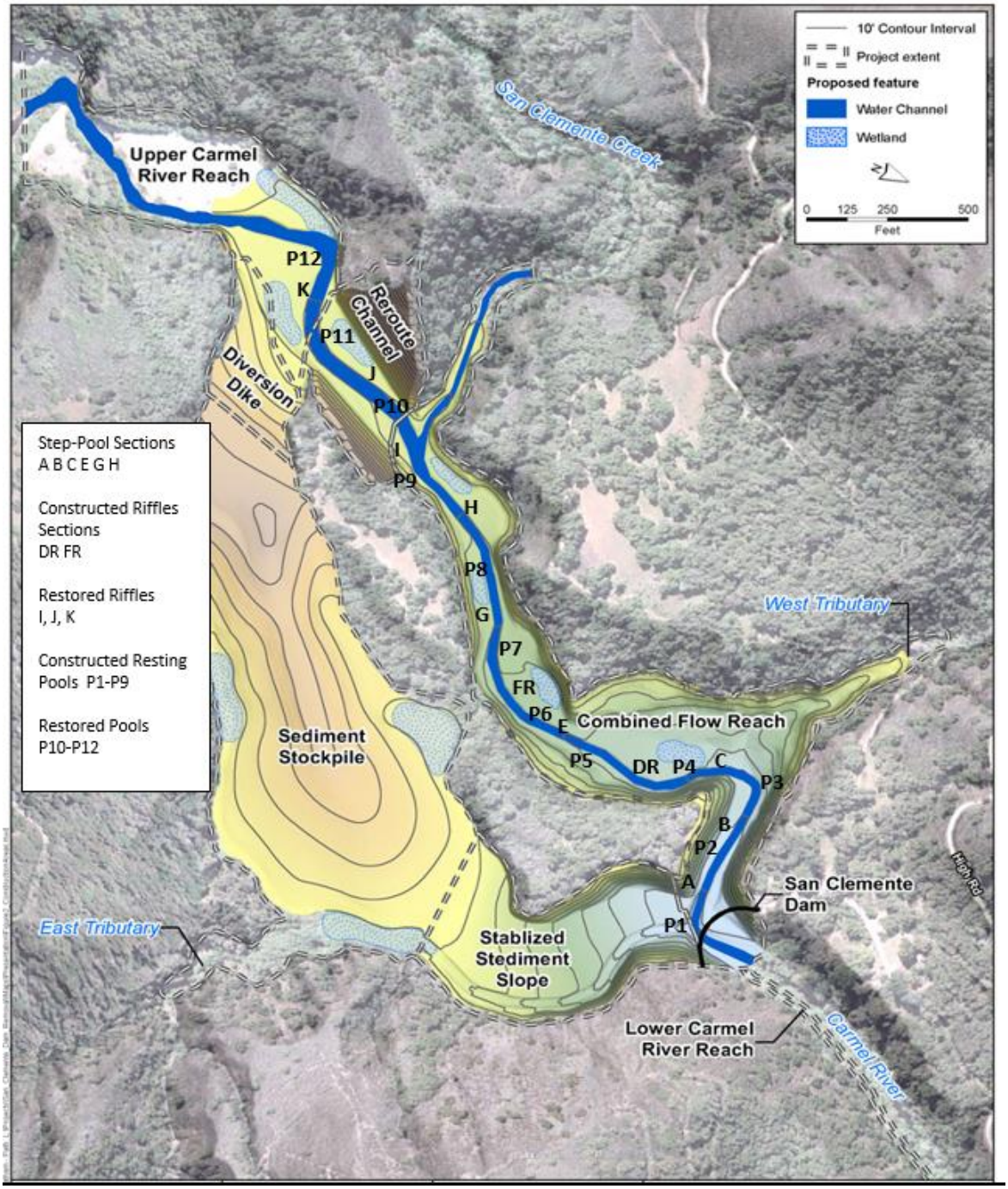

Figure 4: Specific design reaches and elements assessed in this report. Base map from URS (2012).

In the combined flow reach, there are 53 berms distributed in eight step-pool sections. Each section of step-pools is separated by a large steelhead resting pool that ranges from 75 to 105 feet in length (Fig. 5; Tetra Tech, 2015). The building blocks for the step-pool berms include specifically named structural

boulders (Fig. 6). Collectively, they are deemed the “crest nucleus boulders” (CNB). They provide stability to the berm based upon their size and placement. The outermost boulders of the berm are called the key boulders and the boulders next to those are called the notch boulders (Fig. 7). The crest boulder is located in the center and is mostly flat on top. At low flows, the crest boulders allow fish to easily swim up and over the berm to travel upstream. In map view, these boulders are arranged in a structural arch to prevent any boulders from moving forward under high shear stress (Fig. 7). The downstream concave arch also acts to focus strong flow toward the central scour pool, and away from FES and bank materials. The crest boulder acts as the top of the arch, and the stresses are transmitted laterally to the bank through the notch and key CNBs.

Figure 5. Representative photo of constructed step-pools in the combined flow reach. Oblique aerial upstream view. Step pool sections A and B are shown, separated by pool 2.

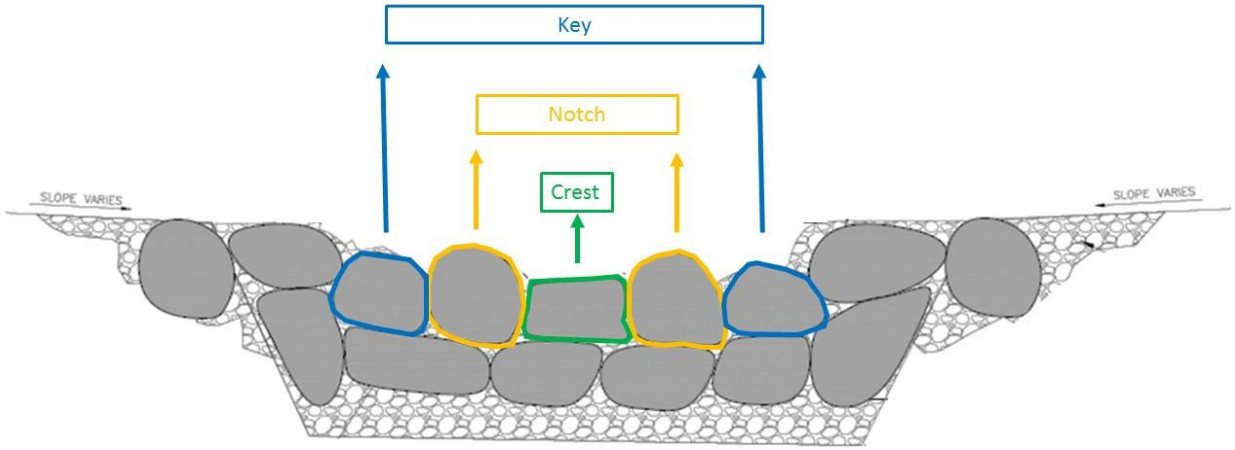

Figure 6. Diagram of CNB – Types of Boulders Labeled. (Modified from Tetra Tech 2015).

Figure 7. Downstream view of berms in section E. In general, berms were constructed with an arch shape for structural stability and to concentrate the hydraulic stresses toward the middle of the channel. Channel and constructed banks are in excellent condition following one season of flow.

The reroute reach is located upstream of the combined-flow reach. It is a low-gradient, meandering section of river that was placed in a gap excavated from the ridge separating San Clemente Creek from the original Carmel River route. It includes a pilot channel with pools and riffles (Fig. 8).

Figure 8. Representative photo of constructed riffles and pools in the reroute reach. Oblique aerial downstream view. Elements shown include pools 9, 10, and 11, and riffles I and J. Section H step-pools are in far background, downstream of resting pool 9.

While the combined flow reach and reroute reach were both constructed using active restoration techniques that create strong physical boundaries for the bankfull channel, the Upper Carmel River Reach was constructed with a pilot channel through poorly consolidated floodplain materials (Fig. 9).

Engineered stream banks are another important aspect for overall CRRDR project success. The banks need to be stable enough to resist erosion during large flows. Roots from vegetation help to stabilize soil and dirt on the banks of natural streams. But, before new plants can supply strength, the project relies upon wrapping the banks in fiber encapsulating soil (FES). The FES is tightly compacted and anchored to key rocks in the bank (Fig. 10). Fiber matting is tightly wrapped around the soil and staked in place with a great number of wooden stakes and live stakes (Fig. 11). The assumption is that the riparian plantings will supply the bank strength by the time the fiber matting biodegrades.

Figure 9. Oblique aerial view upstream of Upper Carmel River Reach. Broad pilot channel was constructed within floodplain deposits. Large woody debris structures were installed on the floodplain.

Figure 10. Soil compaction during FES installation.

Figure 11. FES upstream from San Clemente Creek after the winter runoff showing healthy riparian plantings and a veneer of fine sediment from the first overbank flows.

Large Woody Debris (LWD) adds hydraulic roughness and habitat complexity to natural floodplains. In this project a great number of strong large wood structures were deeply anchored to the floodplain for those purposes—to slow floodwaters and to create diverse habitat opportunities for riverine wildlife (Fig. 12).

Figure 12. LWD installation on left floodplain downstream from San Clemente Creek. Fiber matting was used to protect unvegetated floodplain soil from erosion until flood deposits and pioneer vegetation do the job.

Various design elements of the constructed reach of Carmel River were designed to survive flows categorized by the flow recurrence interval (Table 1). In-channel features, such as crest nucleus boulders and large woody debris structures on the floodplain, undergo varied amounts of hydrologic force depending on their position in the valley. Each feature was designed to withstand a certain flow magnitude designated by recurrence intervals calculated from nearby stream gages or modeling. A long term monitoring study can effectively analyze the evolution of the stream channel, using these guidelines for the expected stability of each in-channel feature.

Table 1. Design requirements for the stability of project features (Tetra Tech 2015).

Project Features	Recurrence Interval (years)	
CNB	50	
Channel Banks	25	at step crests
	5	at other locations
LWD	10	

1.4 Monitoring Impacts of San Clemente Dam Removal

This dam removal is unique because it sequesters the stored reservoir sediment on site rather than allowing it to flow downstream. Because the sediment will stay on site, the environmental impacts of the dam removal are predicted to be negligible. A long term monitoring project has been initiated to record short-term and long-term changes in the Carmel River that result from the dam removal. The overall collaborative study includes before-and-after, and above-and-below impact experimental design (Boughton et al. 2016). The measured variables include an array of fish utilization metrics, turbidity, cross sections, substrate analysis and large wood inventories. Some of the "before" removal data sets are available in technical reports (Chow et al. 2016; MacCarter et al. 2016; Beck et al. 2013). Previous studies include the recruitment of large wood (Beck et al. 2013) and changes in the geomorphology of the new designed channel (Chow et al. 2016). This report is the first to monitor the changes that occur in the constructed bypass channel and floodplain.

2 Fluvial Geomorphic Theory

A river is a dynamic system that changes readily throughout geologic time (Schumm 2005). Natural river channels in steady-state equilibrium (e.g., Ritter et al. 2011) preserve their average geometry while transporting their sediment load without net aggradation or degradation (e.g., Leopold and Bull 1979), as measured over a time frame commensurate with the physical scale of the river (Howard 1982). Therefore, it is understood that constructed river systems will continuously adjust through time. We can learn about the timescale and magnitude of those adjustments through long-term monitoring of river anatomy. A constructed river offers a large-scale experiment in physical river processes. The fluvial geomorphic terms used in this report are defined below.

2.1 Dimension

The dimension of a river is the bankfull cross-sectional area of the channel, and is determined by discharge, sediment size and type, and stream bank materials (e.g., Rosgen 1996). The bankfull discharge is "considered to be the channel-forming or effective discharge" (Leopold 1994) and transports the largest cumulative sediment load (Ward et al. 2016, Wolman and Miller 1960). Table 2 defines the main components of channel dimension.

Table 2: Cross sectional and sedimentological dimensions.

Cross Section Element	Definition	Typical Symbol
Width	width at top of channel	W_{bkf}
Area	Sum of polygonal area formed by the survey verticals, channel bottom, and the bankfull elevation.	A_{bkf}
Depth	Average water depth	$d_{bkf}= A_{bkf}/W_{bkf}$
Width/ Depth Ratio	A measure of stream aspect ratio and has to do with the streams ability to transport water and sediment.	W_{bkf}/d_{bkf}
Wetted Perimeter	Linear distance that is in contact with water at bankfull conditions.	WP
Hydraulic Radius	Measure of stream efficiency	$R=A_{bkf}/WP$
D_{16}	16^{th} percentile of grain size	D_{16}
D_{50}	Median Grain Size	D_{50}
D_{84}	84^{th} percentile of grain size	D_{84}

2.2 Pattern

Channel pattern is known as the “plan view”, because it is the meandering, braided or reasonably straight path of the channel as seen from above (e.g., Rosen, 1994). Channel pattern is controlled by several interacting variables (Leopold and Wolman 1957). The degree to which a stream meanders, or sinuosity, is defined as the ratio of stream length and valley length. Other parameters are meander wavelength, radius of curvature, belt width and amplitude (Fig. 13, Table 3; e.g., Rosgen, 1996).

Table 3: Planform Geomorphic Elements

Pattern Element	Definition	Typical Symbol
Meander Length	Average valley length between full meander loops	Lm
Valley Length	Length of valley measured along direction of fall of valley	Lc
Radius of Curvature	Radius of circle that approximates the shape of a meander loop	Rc
Sinuosity	Ratio of channel length to valley length (Lc/Lv)	K
Meander Belt Width	Width of corridor containing the meander pattern	Wb

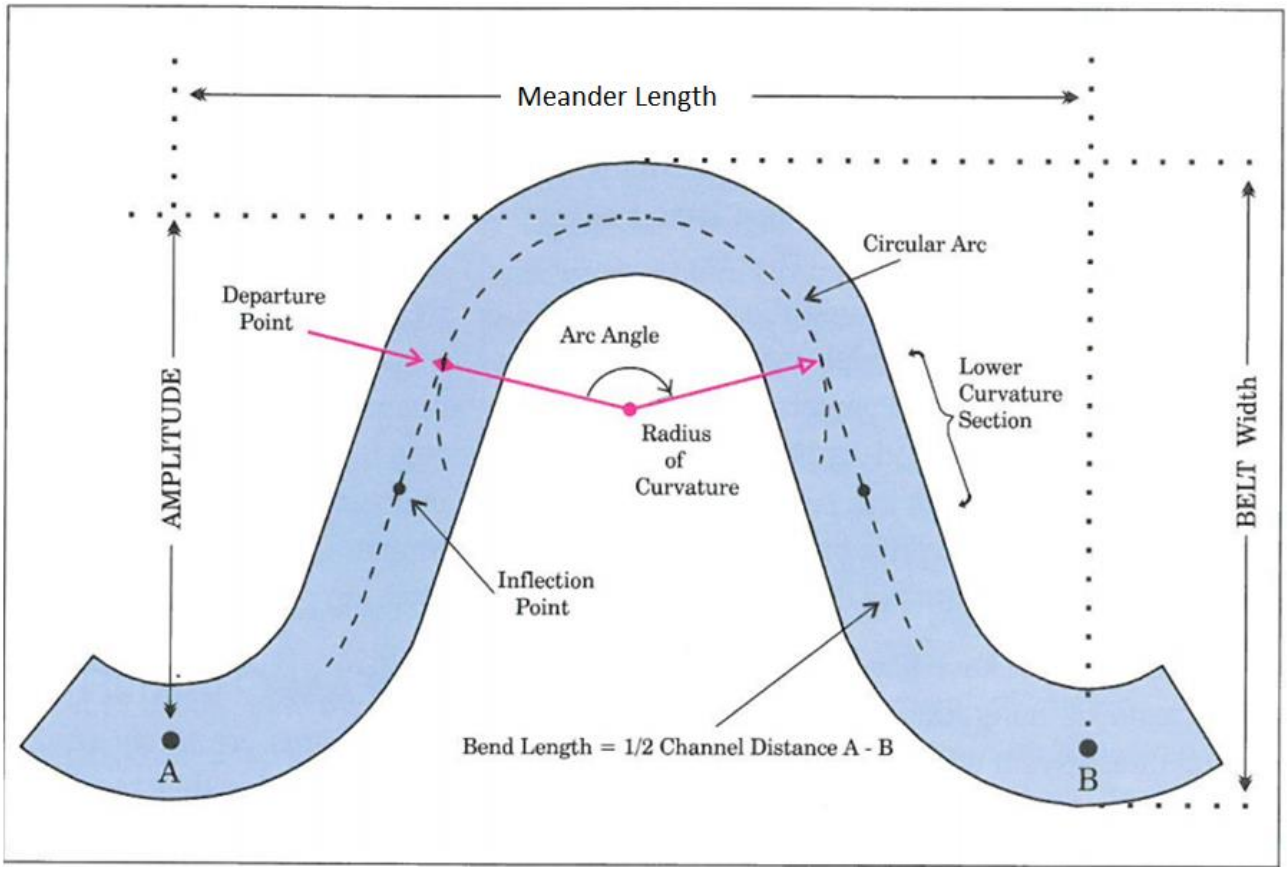

Figure 13. Typical planform geomorphology (Reproduced with permission from Rosgen 1996)

2.3 Profile

The river profile is its down-valley longitudinal slope, measured by the vertical change in elevation divided by the horizontal distance. Valley slope is inversely related to sinuosity of the rivers flowing through the valley: a channel slope of 2% or greater results in step-pool systems with low sinuosity, and channel slopes of less than 2% result in more meandering rivers with wider floodplains (Rosgen 1994).

2.4 Dimensionless ratios in fluvial geomorphology

Leopold et al. (1964) recognized that the various anatomical parts of a river are interrelated, and worked to classify their relationships in stable, low gradient rivers. Leopold et al. (1964) found that low-gradient rivers, independent of scale, have meander lengths that are approximately 11 times their bankfull widths (Fig. 14). Meander length is 10-14 bankfull widths apart (e.g., Ward et al. 2016) and riffles, pools, and point bars are 5-7 bankfull widths apart. These, and other dimensionless scaling ratios, are commonly used to design river construction projects.

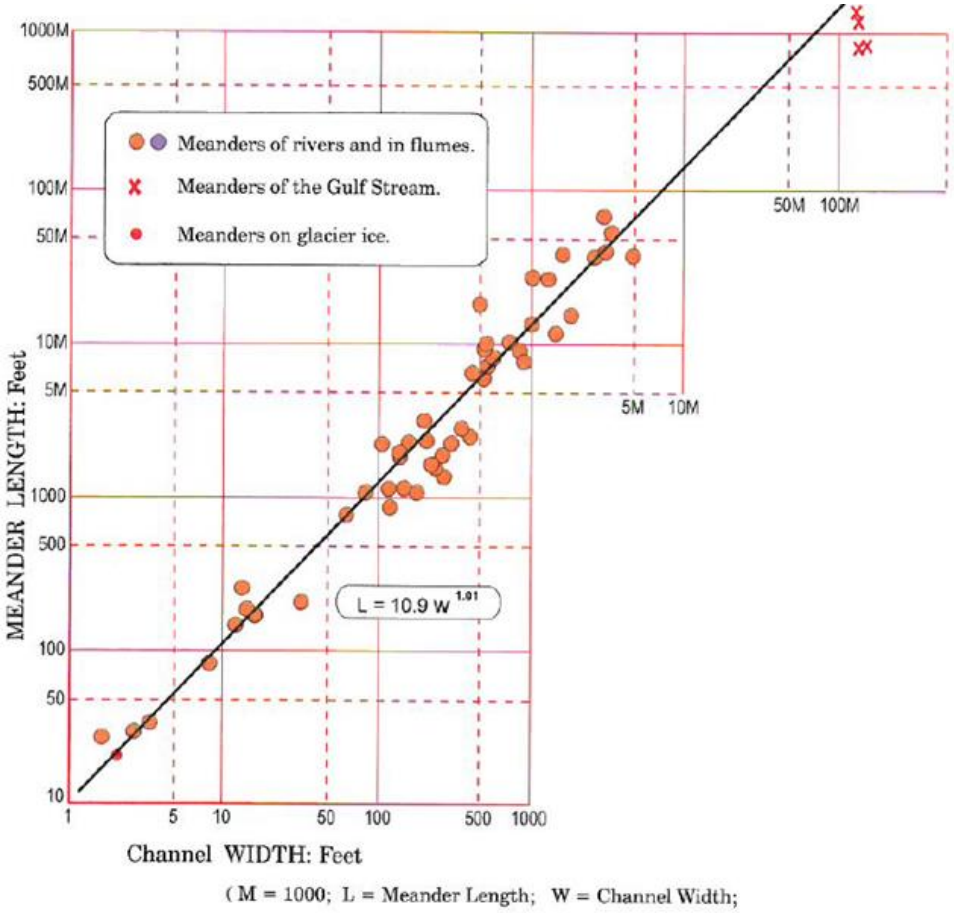

Figure 14. Scatter plot of meander length as a function of stream width. Figure was first published by Leopold et al (1964), and was reproduced here with permission from Rosgen (1996).

Rosgen (2006) created a scatter plot of naturally-stable channel reaches showing that steeper slopes give rise to shorter pool to pool spacing, for a given bankfull width (Fig. 15).

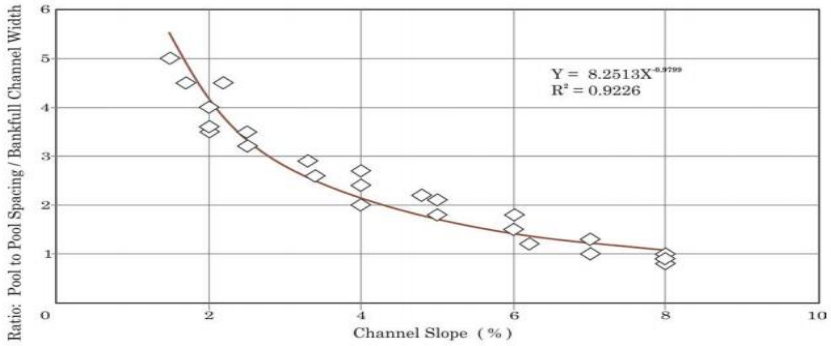

Figure 15. Scatter plot stable step-pool channels showing variability of pool-pool spacing normalized to bankfull width as a function of slope (Reproduced with permission from Rosgen (2006)).

Chartrand et al. (2011) examined the geometric structuring of alluvial step-pools (Fig. 16), and found that the newly created parameter, aspect ratio (α), varies inversely with slope and is able to describe step wavelength and height. The aspect ratio is defined as stream width (Wa) divided by step drop height (Zs). Step wavelength (λs) and step height (Hs) were graphed as a function of α after being normalized by step drop height (Fig. 17). Using characteristics of both stable and unstable natural streams, the resulting plots show a linear relationship with considerable scatter between the variables in log-log space.

A practical application of diagrams like Figure 15 and 17 is to differentiate unstable stream reaches from stable stream reaches, as an aid to designing and constructing stable systems. Figure 15 has no unstable step-pools plotted for comparison. Figure 17 has one unstable example plotted, but it is not distinguishable from the scatter of points depicting stable streams.

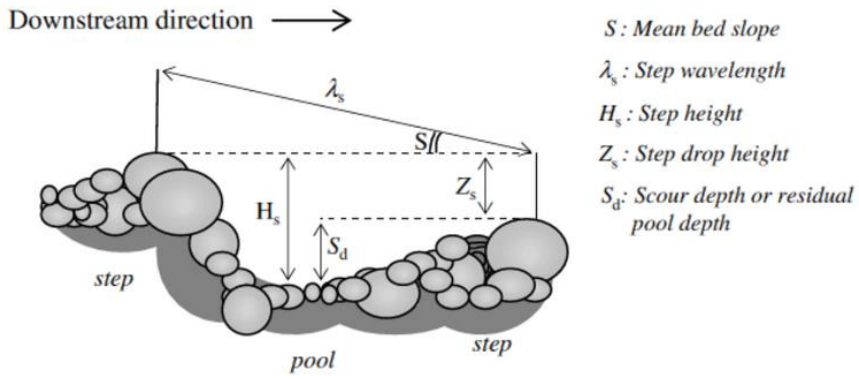

Figure 16. Longitudinal profile of a step-pool sequence with channel morphology terms defined (Reproduced with permission from Chartrand et al. 2011).

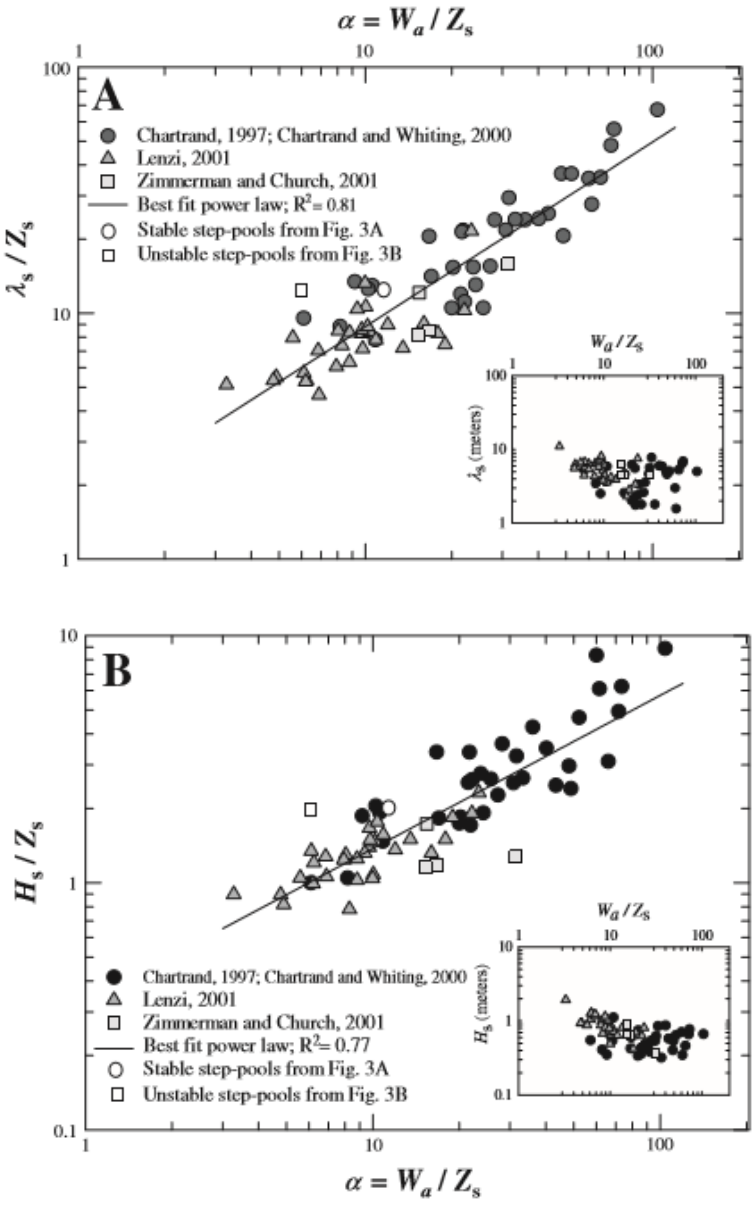

Figure 17. Two scatter plots (A and B) of dimensionless ratios measured on naturally stable step-pool channels and one unstable channel (Reproduced with permission from Chartrand et al., 2011).

3 Goals

The newly constructed channel and floodplain system that replaced the San Clemente Dam offers the opportunity to learn how constructed river systems evolve through time, and how well specific design targets are met. The project was constructed in late 2015, in time to carry the winter runoff of water year 2016. The overarching goal of our work was to assess the project performance following that first year of operation, and to set standards for monitoring through additional years.

To accomplish that work we completed the following tasks with 12 students in 2.5 days of fieldwork plus followup laboratory and analytical work.

1) We analyzed hydrologic data to determine magnitude and frequency of flows that impacted the project area.
2) We walked the length of the channel, locally noting the kind and magnitude of geomorphic change.
3) Following the visual assessment, we investigated reasons for the observed changes.
4) We surveyed benchmarked cross sections to compare with design blueprints, and as a baseline for detecting future change. We also compared the cross sections to local, regional and general reference rivers.
5) We analyzed particle count data to assess sediment transport and as a baseline from which to measure future changes.
6) Lastly, we developed a summary map to communicate the general changes that occurred during the first year, and compared those changes to performance criteria specified in the construction plans.

4 Methods

4.1 Hydrologic conditions during WY 2016

Two standard methods for calculating local stream flow frequencies are through annual maximum series and partial duration frequency. The differences in frequency are not significant for events with recurrence intervals greater than ten years (Dunne and Leopold 1978). In this study we use standard partial duration methods to accurately determine the recurrence interval of the storm runoff events that occurred during the study period because they were low magnitude events. We compare those results with those estimated using the annual maximum series, and estimates published in the Tetra Tech (2015).

For partial duration series discharge data were obtained from the USGS gage Carmel at Robles Del Rio from October 1, 2007 to April 26, 2016 (USGS 2016). Independent hydrograph peak events were defined as those that had an initial discharge near base flow and that exceeded 700 cfs. Events were not used if they either did not exceed 700 cfs or did not initiate the rising limb from base flow.

4.2 Reconnaissance visual assessment of geomorphic change

To assess the first year of change in the Carmel River Reroute Project, we visually compared conditions in early April 2016 to photographs that were shot in 2015, shortly after the project was completed. We walked along the constructed channel and used the photographs to note any changes that had occurred during the first year of runoff. After collecting our field data, we digitally annotated aerial photographs provided by California American Water Company, using a color-coded system to depict various changes. Transparent colored polygons were used to indicate different mechanisms of change (Fig. 18). Large woody debris was denoted with wood shape clipart, depositional features were denoted with transparent yellow polygons, missing or significantly altered features were denoted with red transparent polygons, moderately altered features were denoted with transparent orange polygons, new stream channel routes were denoted with light blue transparent polygons, and when important, the original channel route was denoted with transparent

green polygons. This analysis was completed for the entire constructed channel, including the Upper Carmel River reach, the reroute channel, and the combined flow reach.

Figure 18. Visual assessment key.

We also created a Likert numbering scale that rated the visual condition of the project (Appendix A). As we walked along the constructed channel, we used our scaling system to rate the condition of various important features of each section. The scaling system was different for each individual feature that we were interested in evaluating. For example, we assessed the condition of the bank at each section by ranking it as a 1, 2, or 3. A rank of 1 means that the bank was highly altered from original conditions, a rank of 2 means that the bank was damaged, and a rank of 3 means that the bank was in good condition. We considered a highly-altered bank to be one that had been completely eroded away and no longer looked like the original constructed channel. We considered a damaged bank to be one that was not completely eroded, but would likely become damaged in the next major flow event. A bank was considered to be in good condition if it was still structurally sound and resembled the original constructed bank in the photographs.

The Likert scores were summed and we tested for statistical relationships between the scores for soil lifts (FES) and the local slope of the channel. Categorical assessment scores collected at the site and binned slope data from the construction plans were used in a Chi-Squared test. In order to perform this statistical analysis, the continuous data for slope needed to be transformed into categorical data, as well. The raw slope values were plotted against the damage coefficients. The trends that we saw in slope were then categorized into four

distinctions based on an arbitrary range. The ranges included; “High” for slopes of 5.5-4.5 percent, “Medium” for values between 4.5 and 3.5 percent, 3.5-2.5 was named “Low”, and any value below 2.5 percent slope was named “Very Low”.

4.2.1 Investigations of CNB instability

The step-pool berms were designed to remain stable in flows up to the 50 year event (Tetra Tech 2015). Initial visual assessment indicated that some CNB boulders had moved, so we investigated the conditions that may have led to movement.

4.2.2 CNB Density

As is standard practice, the critical boundary shear stress required to move the CNBs was calculated assuming the rocks had the average density of granite 2650 kg/m^3 (Tetra Tech 2015). However, the berms were constructed of sandstone blocks, which might have a different density. We estimated the density of the sandstone used in the project to determine if there is a notable difference in the density between the two rock types. We expected that the sandstone porosity (or pore-filling cement) of the sandstone would decrease the density, and thus the amount of shear stress required to move the berm-forming CNBs (Nicol et al. 2014).

We retrieved sandstone samples from the Carmel River site and broke them down into measureable pieces (Fig.19). The following methods estimate the density difference between the water-saturated sandstone samples, and a synthetic granite rock: a rock where the sandstone framework grains and porosity are both assumed to have quartzo-feldspathic density (2650 kg/m3). The approach is to determine the porosity volume of water-saturated sandstone, then analytically swap the water in the pores with granite.

Figure 19. Sandstone samples used to determine density of CNB block

We soaked the samples for at least 72 hours, blotted the surface water, and determined the mass of the water saturated sample (Mw) using an analytical balance. We then oven dried the samples at 100 C, until subsequent mass measurements did not change, indicating a fully dried sample (Md). The difference between wet and dry sample mass is the mass of the pore-filling water:

$Mw - Md = Mw$

Then,

$Mw / \rho w = Vw,$

where ρw is the density of water, and Vw is the volume of water. The volume occupied by framework sandstone grains (Vg) is

$Vg = Md / \rho g ,$

where ρg is the density of the quartzo-feldspathic grains, 2650 kg/m^3. We then computed to mass of an equivalent piece of granite by applying the mass of granite to the total volume of the sample.

$Mg = (Vw + Vg)\ \rho g$.

We then calculated the % difference between the mass of the saturated sandstone (Mw) and the mass of the synthetic granite (Mg). We also calculated the bulk density of the water-saturated sandstone (ρss).

$\rho ss = Mw / (Vw + Vg)$.

4.2.3 CNB Shape

Sedimentary particles, including the large boulders used to construct the berms, will move more easily if they have a higher drag coefficient. Drag coefficient is related to particle shape. The CNB were modeled for stability assuming they were spheres that initially moved by rotating forward over a 0.3 ft high fulcrum, but the CNBs are actually blunt rectangular solids. We explored the impact of that geometric difference in the literature.

4.2.4 Fluvial geomorphic relations for step-pool design

Premature adjustment of the step-pool berms and CNB elements could be caused by design parameters that are inappropriate in some way. Various design elements were plotted on published scatterplots that depict the dimensionless geometry of naturally stable streams. Design elements that do not conform to stable streams can be discerned by comparison to the scatterplots. For this work we used plots of various dimensionless step-pool morphology variables (Figs. 15 and 17).

Rosgen (2006) variables (Fig. 15) were directly measured from design blueprints, whereas Chartrand et al. (2011) variables (Fig. 17) were previously calculated and plotted by Tetra Tech (2015). We recalculated and plotted the step-pool geometry after splitting the data into 3 slope category ranges.

We also surveyed and plotted a reach of unstable step-pools in Monterey to test the discrimination power of the Rosgen (2006) and Chartrand et al. (2011) dimensionless plots.

4.3 Comparison of blueprint drawings to channel morphology

Six benchmarked cross-sectional surveys were established along the reroute channel (Fig. 20). Rebar benchmarks were installed on the right and left banks and were marked with an orange benchmark cap. Coordinates of each right benchmark were measured using RTK GPS to ensure the relocation of the benchmarks in future studies. Cross-sectional surveys were conducted in accordance with techniques described by Harrelson et al. (1994). We used auto levels with tripods, transect tapes, and survey rods.

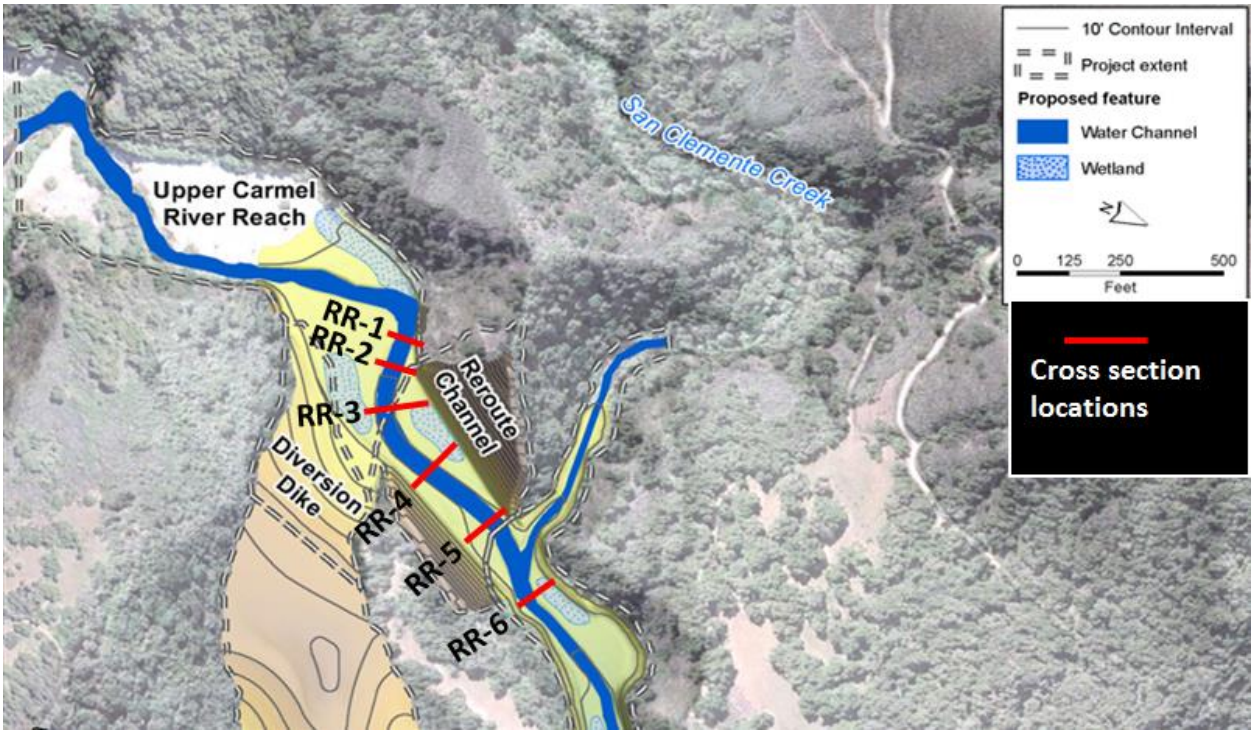

Figure 20. Locations of benchmarked cross sections. Base map from URS (2012).

We re-projected the project blueprint drawings from CA State Plane FIPS IV (feet) to NAD 83 UTM (meters) in ArcGIS v.10.2.2 to match the coordinate system for our cross section benchmarks. Using the benchmark locations as a guide, distance and elevation points were read from the blueprints where the transects crossed blueprint contour lines in Arc GIS. Blueprint elevations were manually increased by 0.877 m to adjust for the local difference between vertical datum NGVD 29 (blueprint) and NAVD 88 (our surveys). The resulting x,y points were plotted with no further adjustment on top of the surveyed cross

sections. Comparisons were made both visually and through calculated cross section geometry (see section 2.1).

4.4 Comparison of channel morphology to regional reference channels

Bankfull dimensions were taken from riffle cross sections surveys with corresponding GIS blueprint data for the same cross sections, and from control reaches upstream from the CRRDR project site. Area, width, depth, width/depth ratio were calculated for bankfull stage determined from graphs or notes. The data were then plotted by drainage area on previously published graphs of bankfull geometry from the broader region (Hecht et al. 2013).

4.5 Comparison of channel substrate to local reference channels

We compared the channel sediment size distributions upstream of the project to those within the project. We conducted particle counts on point bars and at the 6 cross sections described above.

We conducted particle counts on four major point bars that had formed in the project. The point bars spanned from upstream of pool 12, near the upstream end of the project to downsteam of pool 1 at the lower end of the project. We created an (x,y) coordinate system at each point bar to conduct a random sample. The y-axis ran the length of the point bar, while the x-axis spanned the longest width (Fig. 21). We accounted for the variation of point bar widths by taking the sample at the outermost edge of the point bar if the x-coordinate was past its bounds.

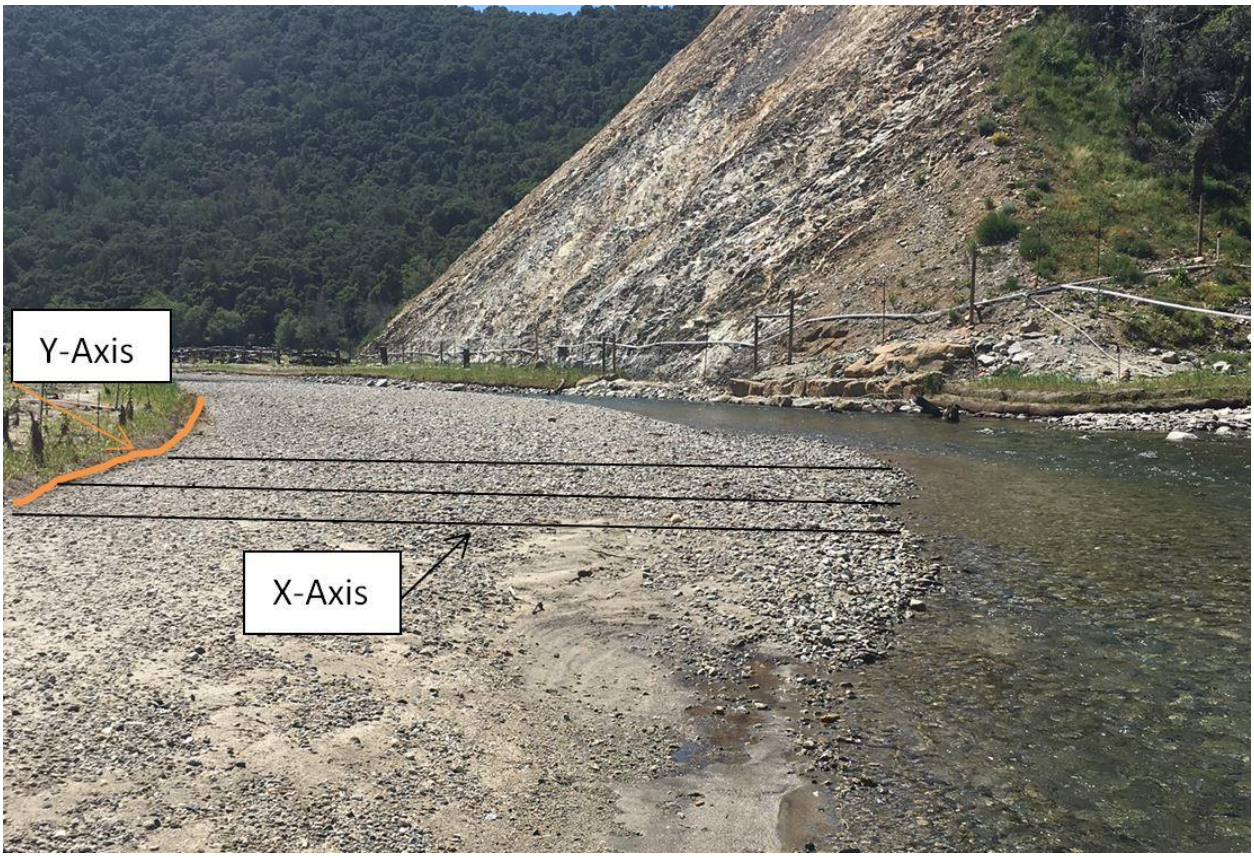

Figure 21. Point bar near the mouth of San Clemente Creek. Lines show showing how the sampling grid was constructed.

We randomly selected ten (x,y) coordinates using a random number generator. We took ten samples at each (x,y) coordinate using a 0.5 m quadrat, making a total of 100 measured particles at each point bar. Particles were classified into class sizes by their intermediate axis using a gravelometer that replicates sieving and reduces error (Fig. 22).

Figure 22. Pebble count using a half-meter quadrat and gravelometer.

We also conducted particle counts at cross sections 1-6. We measured the distance between left and right bank FES and divided by 100 to obtain the distance for 100 particle measurements. We used a gravelometer to record each particle chosen from the streambed without bias to its particular size class.

We completed graphical analyses on all particle count data. Cross section and point bar reach totals were used to calculate the cumulative percentage of pebbles that were finer than each size class. Graphs of the cumulative particle size distribution were created for the cross sections and point bars to analyze particle size in different reaches of the river. From these graphs we determined the 16th percentile (D_{16}), median sediment size (D_{50}), and the 84th percentile (D_{84}). Histograms of particle size frequency were also created to compare sections. These initial particle counts will provide the baseline for future monitoring and comparison of channel substrate.

5 Results

5.1 Hydrologic conditions during WY 2016

The river project success criteria include an estimate of the flow magnitude that various design elements would withstand (Table 1). We estimated the recurrence interval (RI) of the two main runoff events that occurred during the study period to give the first-year assessment context (Fig. 23). The peak discharge values at the Sleepy Hollow gage are likely close to the values at the project site because of the proximity of the gage. The Robles del Rio gage was used of flow frequency analysis because of the longer record (Fig 24). The peak discharge values for the events were greater at Robles del Rio than at Sleepy Hollow or the project site; however, we assume that the frequency of those peaks would be the same, since the gages are not exceptionally far from each other, and the peaks represent the same magnitude rainfall events, interacting with the same antecedent moisture conditions within the same watershed.

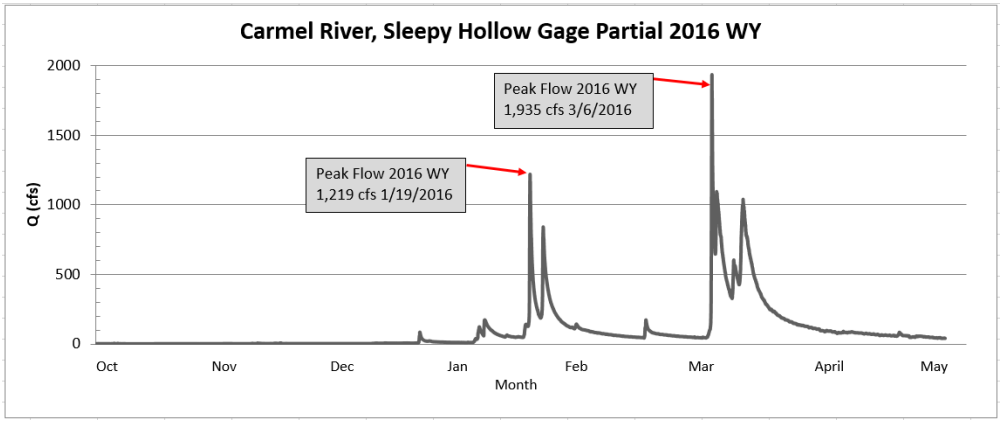

Figure 23: Hydrograph for a part of WY 2016 winter runoff at the Sleepy Hollow gage (Fig. 2). The two main discharge peaks for the year are labeled.

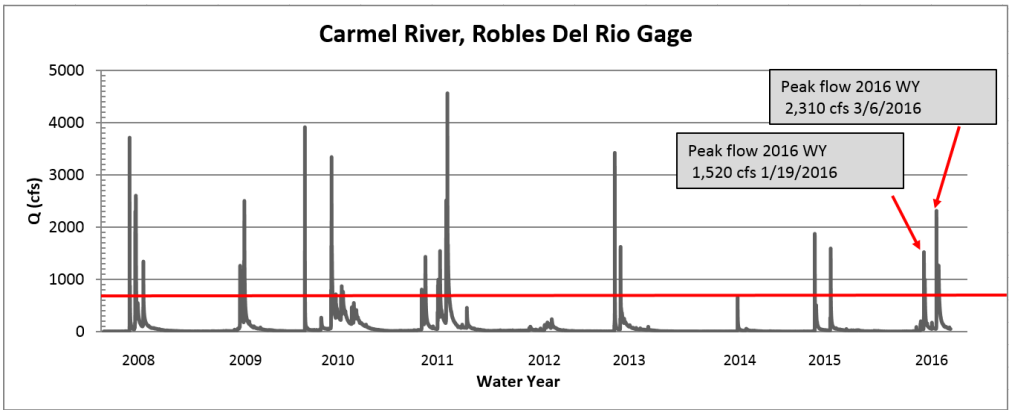

Figure 24. Hydrograph from Robles del Rio gage (Fig 2). As in Figure 23, the two highest flows during the study period are indicated. The red line is the 700 cfs threshold we used for partial duration series analysis.

Both partial duration and Log-Pearson-III analyses were made for comparison. For partial duration analysis, 20 independent events exceeding 700 cfs were identified in the most recent 9 years of the Robles del Rio USGS gage record (Fig 24). The peak flow events were ranked and assigned Weibull recurrence intervals (Table 4). The first of the two runoff events for the study period occurred on 1/19/2016. It had an RI of 0.8 years. The second event occurred on 3/6/2016, with an RI of 1.4 years.

The design report estimated that the RI for the 3/6/2016 and 1/19/2016 events at the project site were 1.7 years and 2.9 years, respectively (Table 4). Log Pearson-III analysis of the annual maximum series of the Robles del Rio gage indicates that the peaks had RI values of 1.5 years and 1.9 years respectively (Table 5).

Table 4. Partial Duration Frequency Analysis for Robles Del Rio. Yellow marks the 2016 water year peaks.

Date	Q	Rank	RI
3/24/2011	4560	1	10.0
10/14/2009	3910	2	5.0
1/4/2008	3710	3	3.3
12/2/2012	3420	4	2.5
1/28/2008	2600	5	2.0
3/4/2009	2500	6	1.7
3/6/2016	2310	7	1.4
12/12/2014	1870	8	1.3
1/20/2010	1640	9	1.1
12/24/2012	1610	10	1.0
2/9/2015	1590	11	0.91
2/25/2011	1540	12	0.83
1/19/2016	1520	13	0.77
1/2/2011	1430	14	0.71
2/24/2008	1340	15	0.67
2/16/2009	1260	16	0.63
2/19/2011	993	17	0.59
2/26/2010	868	18	0.56
12/19/2010	805	19	0.53
2/5/2010	713	20	0.50

Table 5. Recurrence Interval of WY 2016 peak flows. PD = partial duration series analysis of Robles del Rio gage. LPIII = Log Pearson type III analysis of Robles del Rio gage. Design Report is Tetra Tech (2015).

Event	PDF	AMS LPIII	Design Report
1/19/2016	0.8	1.5	1.7
3/6/2016	1.4	1.9	2.9

The recurrence intervals calculated here using the annual maximum series do not differ significantly from those published in Tetra Tech (2015). Partial duration series analysis provides a more accurate estimate of flow frequency because it employs all the independent peaks of the record, rather than just the single highest flow of each year of the record (e.g., Dunne and Leopold 1978; Smith et al. 2009). The partial duration recurrence intervals calculated here are

certainly overestimates of the true values, since only the most recent 9 years of the record were assessed.

5.2 Reconnaissance visual assessment of geomorphic change

Through our visual assessment of the Carmel River, we found that the constructed river channel has undergone geomorphic adjustments since the completion of the project. Below, we describe the condition of all the river reaches and step-pool sections of the project (Fig. 4) from downstream to upstream, in keeping with the original naming of the section from A to H. In each lettered project section, the berms are named 1 through n in an upstream direction. The images showing change have colors represented in Figure 18 that are plotted on oblique aerial images from a post-construction drone survey by Cal Am. In some cases we show ground-based photography to show more details about the present conditions.

At the downstream terminus of the constructed channel, below Pool 1, the entire floodplain and much of the previous channel is now covered in a thick layer of gravel (Figs. 25 and 26). The main channel has migrated from its original position by eroding the right bank and now runs along the old dam abutment and bedrock on the right side of the channel.

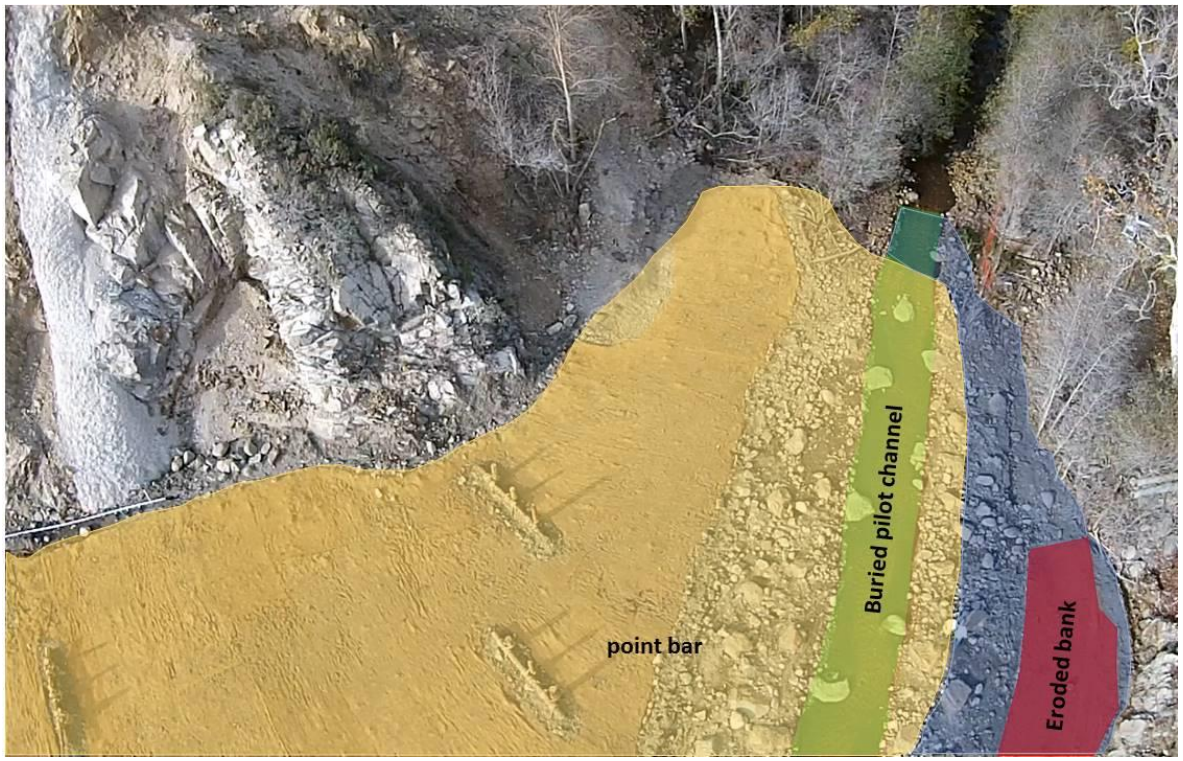

Figure 25. Oblique downstream aerial view at the end of the reroute project where the dam once was.

Figure 26. Downstream view of downstream terminus of the constructed channel. Submerged boulders are the right edge of pilot channel that was buried by gravel bar deposition. Flow eroded left bank and displaced fiber matting to reach bedrock wall near the previous location of right dam abutment.

Upstream from Pool 1, we also saw changes in step pool Section A. Berm A1 was missing, and the CNB boulders were not seen in pool 1 (Figs. 27 and 28). The boulders may have been too deep to be seen. In berm A6 the crest boulder was dislodged and moved approximately 1.2 meters downstream, and the left notch boulder moved about 4 meters downstream. There was a large lateral failure on the right bank from berm A10 to berm A6 (Fig. 29). On the left bank, there was incipient lateral failure and a large amount of FES damage from berms A6 to A10. There were sediment deposits on the left floodplain by A2 and A5 (Figs. 27 and 28). Large woody debris was found on the right floodplain by A3 and on the left floodplain by berms A5 and A7. The upper bank sediment pile on the left bank was eroded (Figs. 27 and 29).

At step pool section B, there was incipient lateral failure present on both the left and right banks of berm B1, with the FES removed on the left bank (Fig. 30). There was a significant amount of sediment deposited on the floodplain between berms B2 and B3 on the left side of the channel. A large lateral failure was present on the right bank from berm B5 to berm B3. A larger lateral failure occurred on the left bank from Pool 3 to berm B5 (Figs. 30 and 31). There were two pieces of large woody debris present in the new channel route. The FES was removed and the seed boulders that were previously on the floodplain were found in the channel because the water eroded the riverbank down to the bedrock.

Figure 27. Oblique upstream aerial view of Pool (lower left) and section A. Berms A1-A10 can be seen.

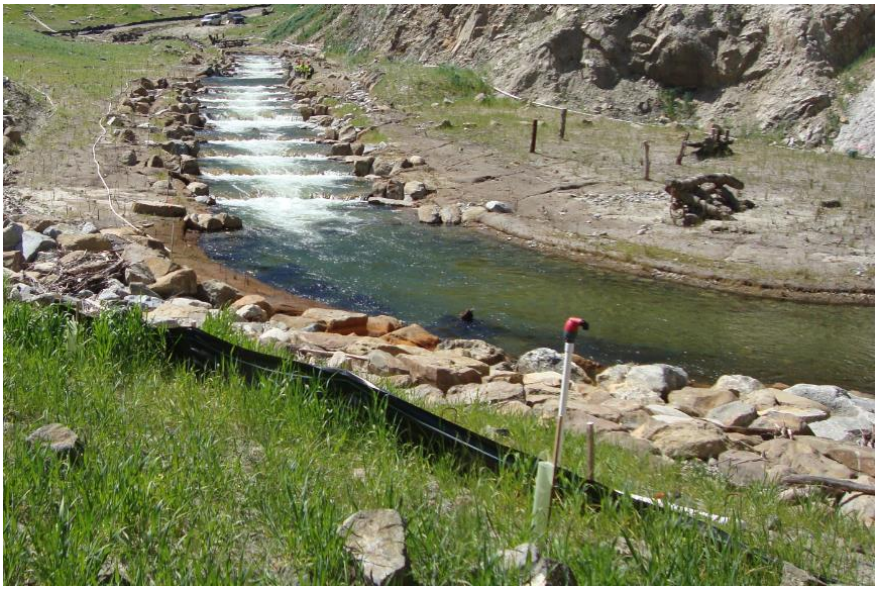

Figure 28. Upstream view of Pool 1 and section A. Banks and FES along downstream end of Section A are in excellent condition. Minor sediment deposition is present on both floodplains. Berm A1 is missing, but step on berm A2 does not appear excessive.

Figure 29. View from right bank near berm A-9. Disturbed FES in foreground is right bank along central section A. Large boulders in background are seed boulders that were partially eroded from constructed upper bank.

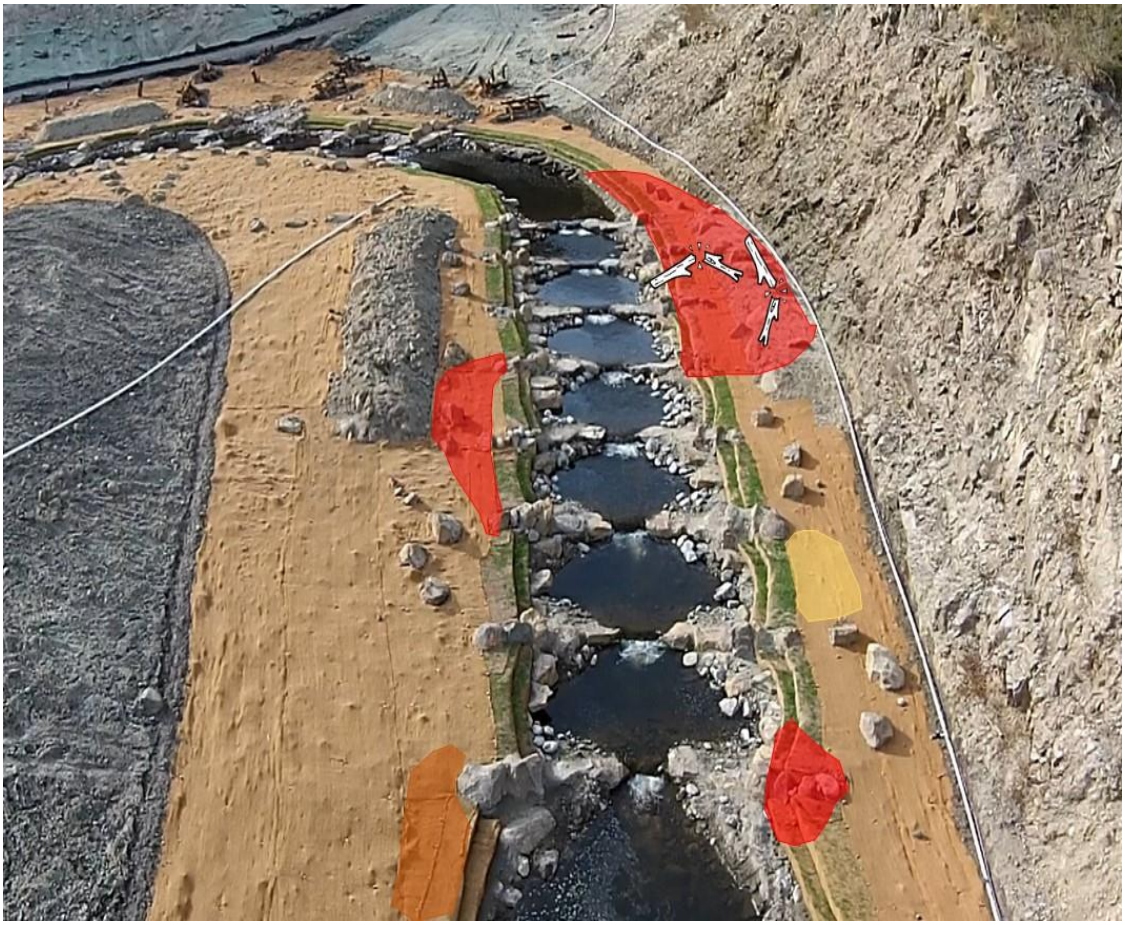

Figure 30. Oblique upstream aerial view of Section B showing berms B1-B8, and Pool 3 at the top of the image.

Figure 31. View of left bank along the upstream end of section B. FES has been removed, and bank was eroded back to the bedrock wall, widening the active channel.

We saw the most structural adjustment in step pool Section C. The left notch boulder in berm C1 was dislodged and moved downstream 4 meters and the left key boulder was moved downstream 6 meters (Fig. 32). The left notch boulder in berm C2 was transported downstream approximately 4.5 meters. In berm C3, the left notch and left key boulders were dislodged and moved downstream approximately 4.2 and 2.5 meters, respectively. There was bank failure from berm C1 to berm C3 and the upper bank sediment pile had been eroded (Fig. 32). The right notch boulder was dislodged from berm C5, but we were unable to relocate the boulder (Fig. 33). In berm C6, the right and left notch boulders moved 2 and 4 meters, respectively. The right key boulder in berm C7 moved downstream about 4.6 meters. In berm C10, the right key and notch boulders both moved downstream approximately 4 meters. There was a lateral failure present between berms C11 and C10 where the right bank and FES were deeply eroded and removed (Fig. 34). There was a deep scour hole along the right edge of the upstream side of C11, potentially indicating piping beneath or alongside the structure (red hatch area in Fig 35; Fig. 36). We also found a significant amount of erosion present on the floodplain of section C where the designed wetlands were supposed to drain back into the river (Figs. 35 and 37), causing a large amount of bank failure from C5 to C7 (Fig. 34). The large upper bank sediment pile along this reach has been eroded (Fig. 33). Large woody debris was present on the right floodplain from berms C9 to C7.

Figure 32. Oblique upstream aerial view showing end of section C emptying into pool 3. Berms C1-C4 are visible.

Figure 33. An upstream view of the upper half of Section C showing berms C3-C11.

Figure 34. Downstream view of FES and bank disturbance on left bank of section C.

Figure 35. An upstream view of Pool 4 and Riffle D. Red cross-hatched area is a deep scour that likely indicates piping below or around the right end of berm C-11

Figure 36. View of C11 from left bank. Note compromised FES on right bank downstream of berm C11. Also visible is the scoured area immediately upstream from the right edge of the berm.

Figure 37. Up-valley view of eroded rocked spillway shown in Figure 18. Knickpoint is visible in upper part of the photo.

A large gravel point bar has formed downstream from Riffle D in Pool 4 (Figs. 35 and 38). We found significant sand deposits starting from that point bar and on the left floodplain, leading to the major erosional feature seen in Figures 35 and 37. A section of the left floodplain near berms C10 and C11 was damaged, with removed FES and significant erosion on the sediment pile. There was also erosion at the top of Riffle D along the left bank and upper bank sediment pile (Figs. 35 and 39). Except for the minor FES adjustment, Riffle D remained stable (Fig. 40).

Figure 38. Upstream view of new sand and gravel point bar on left bank of Pool 4 and downstream end of Riffle D. Note excellent condition of FES and constructed rootwad structures on outside of bend.

Figure 39. Upstream view along left bank of riffle D. Example of modified FES and minor erosion of upper bank immediately upstream of the gravel bar (Fig. 38). Upper bank erosion is expected, and is a source of new gravel for the channel. Erosion location is marked in Figure 35.

Figure 40. Downstream view of stable plane-bed of riffle D. FES is intact on right bank, and moderately disturbed on upper left bank.

Step-pool section E begins above riffle D and Pool 5 (Fig. 4). Figure 7 is a general post-winter view of section E. At berm E3, water cut through the right side of the step (Fig. 43). The FES on the left bank of step E1 was almost removed from the bank. There were large woody debris deposited on the left floodplain. There were gravelly sand deposits in the corners formed by the berm and bank. No changes were seen were seen in Riffle F (Figs 44 and 45).

Figure 2. Oblique aerial upstream view of berms E1–E5.

Figure 44. Post-construction upstream view of Riffle F before winter runoff.

Figure 45. Upstream view of Riffle F after winter runoff. No impacts were noted. There are sand deposits on both floodplains. There is a small side-attached bar growing on left bank. LWD structures, FES, and riparian plantings were in excellent condition.

Section G includes some large woody debris deposits located on the right bank between berms G3 and G4 (Fig. 46). The left notch boulder in berm G2 was dislodged and transported downstream 2 to 3 meters. (Fig. 46).

Figure 46. Oblique aerial upstream view of berms G1-G5. The left notch CNB of berm G2 was displaced.

The FES on the left bank between steps G2 and G5 and between G6 and G7 was damaged (Figs 46 and 47). There are sediment deposits against the upstream edges of the key CNB blocks, most notably on the corner of G4. In general, most of the pool deposition occurred along the right pool banks, while most of the erosion and disturbance was concentrated along the left banks. We found large woody debris on the left bank by G7 and G8 and on the right bank by G6 and G7.

Figure 3. . Oblique aerial upstream view of berms G4-G9.

The right notch boulder of berm H3 moved downstream approximately 4 meters (Figs. 48 and 49). The right notch boulder of berm H4 moved downstream about 0.5 meters. The left notch boulder of berm H6 moved downstream approximately 4 meters. Sandy gravel deposits were filling in the sides of the pools against the upstream side of key and notch CNBs from H1-H3. Pool 9 had large amounts of woody debris (Figs. 50 and 51).

Figure 48. Oblique aerial upstream view of berms H1-H9.

Figure 49. Upstream view of H3. Displaced CNB is visible in channel. This pool is an example showing moderate pool-filling gravel on the right side of the channel. FES in background is performing as designed.

Figure 50. Post-construction downstream view of Pool 9 indicating position of transported LWD structure (see Fig. 51)

Figure 51 . View from right bank at upstream end of pool 9. Transported LWD structure was lodged at head of pool 9. Note intact FES and new riparian herbaceous growth on left bank.

The next section upstream is the beginning of the pool-riffle sequence that spans the upstream end of the combined flow reach and the reroute section of the project (Fig. 3). This reach contains the 6 benchmarked cross sections described later in this study (Fig. 20).

Between pools 9 and 12 (Fig. 4) the pilot channel (Fig. 8) matured into a series of three riffles separated by two point bars with pools (Figs 52-55). In this reach the FES remained in excellent condition. The pilot channel constructed in riffle I migrated to the left bank in response to side-attached bar or point-bar growth near the mouth of San Clemente Creek (Fig. 52). This section also had large woody debris on the point bar (Figs. 54 and 55).

Figure 52. Oblique aerial downstream view of Riffle I, Pool 10, Riffle J, and Pool 11. Pool 9 and berm section H are visible in the distance.

Fig. 53. Cross section RR-4 located in a glide just upstream from the riffle head of riffle J (Fig 4). Surveyors in background mark the location of cross section RR-5 on a point bar and pool 10. FES was in excellent condition.

Figure 54. Downstream view of riffle K, pool 11, and transported LWD structure on point bar. Cross section RR-3 is located along the upstream end of the LWD structure. FES and riparian plantings are in excellent condition.

Figure 55. Oblique aerial upstream view of Pool 11 and Riffle K.

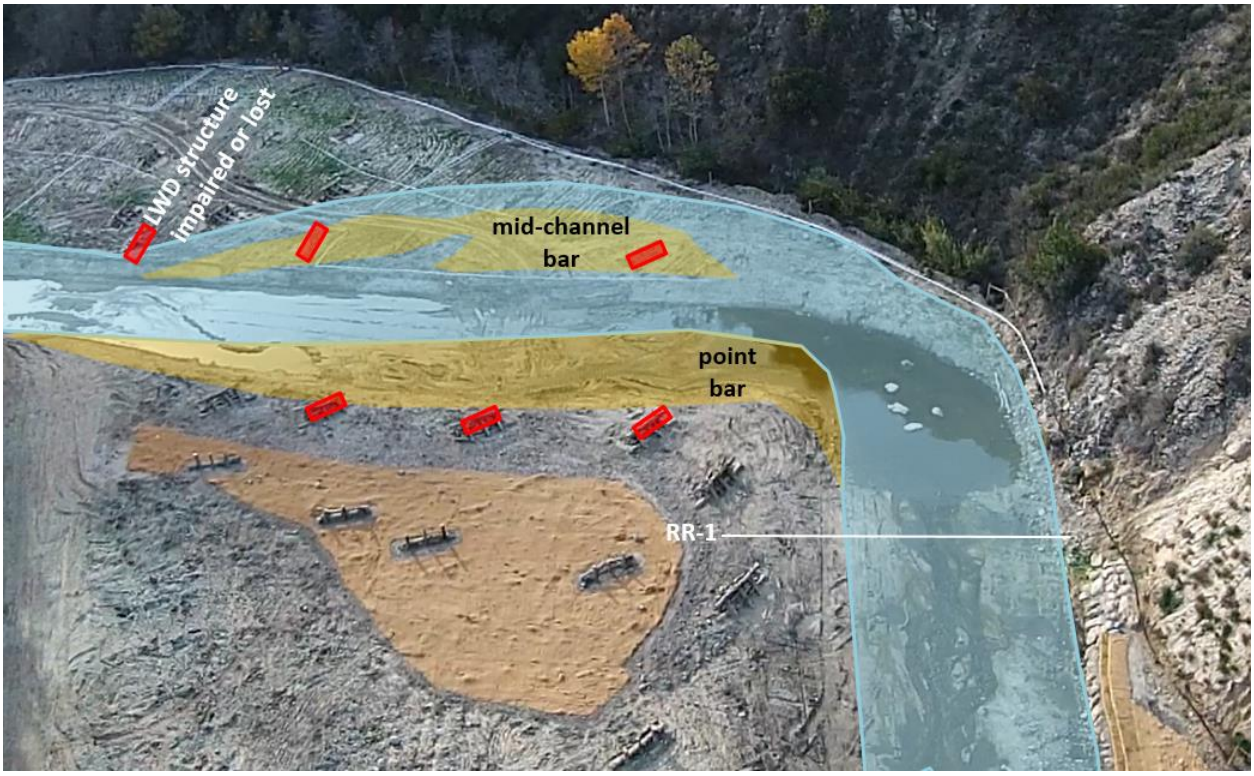

Figure 56. Upstream view of riffle K, pool 12, and the "Upper Carmel" reach. Note lateral erosion of left bank, and growth of in channel gravel bars.

The channel upstream of pool 12 is the unconfined upper Carmel reach (Figs. 56-61). Upstream of pool 12, the channel migrated laterally, cutting mostly on the left bank, and leaving significant gravel bars (Figs 56 and 57), perhaps constructed of the locally eroded material. The radius of curvature (e.g. Fig. 13) of the bend at pool 12 increased substantially (Fig. 56). An increase in stream width led to local incompetence and growth of a mid-channel bar (Fig. 56).

Approximate scaling of the Figure 60 oblique aerial photo, and observation that the eroded floodplain bank was approximately 1.5 to 2 m thick (Fig. 61) indicates that roughly 0.4 acre-ft of gravel was added to the bedload of the river through channel adjustment at the upstream end of the project. That sediment volume is approximately 3% of the estimated 15.2 acre-ft/yr average load (Tetra Tech 2015). Several large wood structures were either missing or structurally compromised (Figs 56-59).

Figure 57. Fish-eye perspective down valley showing point bar growth on right bank adjacent to pool 12, and compromised LWD structures along the same bank. Figure 58 is a close up of one of the compromised LWD structures

Figure 58. Upstream view of compromised LWD structure on right bank upstream from pool 12.

Figure 59. Downstream view of compromised LWD structure now located on mid-channel bar upstream from pool 12.

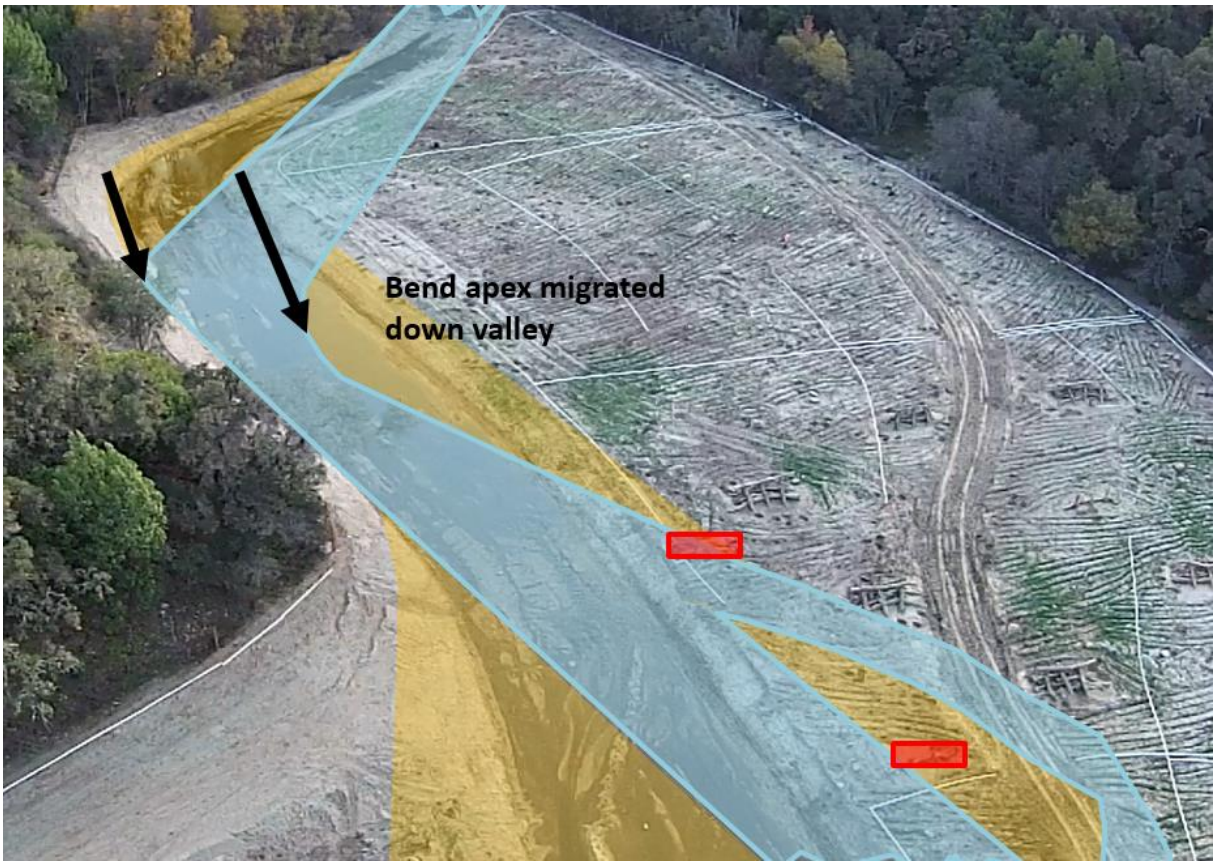

Figure 60. Oblique aerial upstream view of farthest upstream section of the unconfined upper Carmel reach.

Figure 61. Upstream view of eroded left bank in upper Carmel reach. Bank is between 1.5 and 2 m tall. Erosion of this bank released large volume of sand and gravel to channel.

5.2.1 Assessing Likert scale values

Initial assessment of the entire project suggested that the level of alteration of FES and banks was related to local channel slope. To explore that idea, the Likert scale assessment values for each assessment location were plotted with channel slope values (Figs. 62 and 63). A relationship between impaired condition and channel slope is visible in the plots.

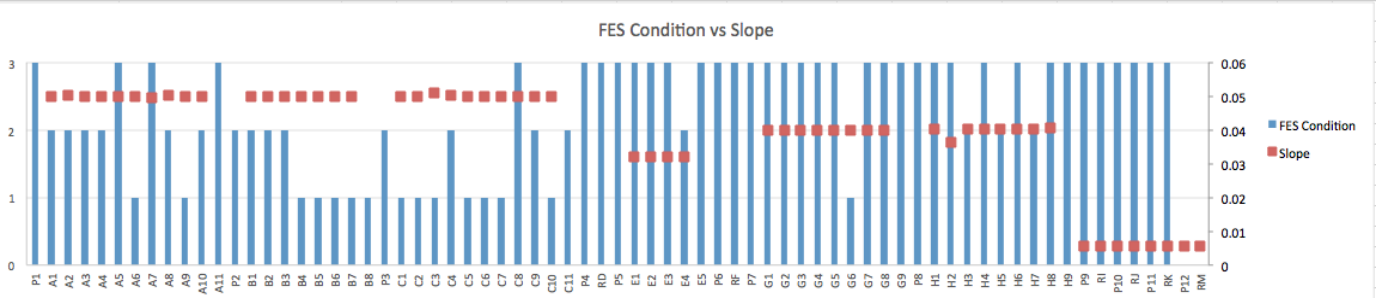

Figure 62. FES condition (blue bars and left axis) and slope (red dots and right axis). Locations on horizontal axis are from Figure 4. Higher values of "condition" represent better condition, with a value of 3 representing excellent condition. Locations are arranged from upstream to downstream from right to left.

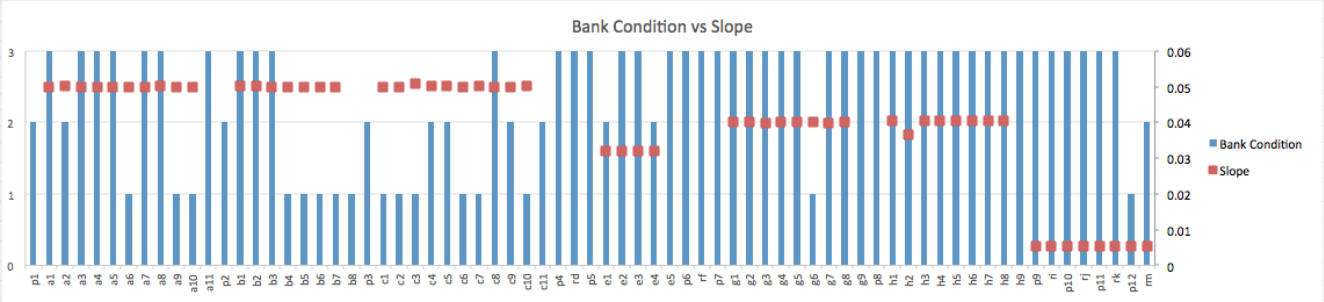

Figure 634. Bank condition (blue bars and left axis) and slope (red dots and right axis). Locations on horizontal axis are from Figure 4. Higher values of "condition" represent better condition, with a value of 3 representing excellent condition. Locations are arranged from upstream to downstream from right to left.

5.3 Investigations of CNB Instability

5.3.1 Density

We calculated the difference between the water-saturated sandstone samples and "synthetic granite" having the same volume. We found an average proportional difference of 4.5% in the mass calculations (Tables 6 and 7). The average water-saturated sandstone density was 2531 $\pm$ 12 kg/m^3 (Table 7). The estimates of lower density for the sandstone samples is conservative, because the actual density of the sandstone framework grains could be lower than assumed (lower than granite). Further, some of the original sandstone porosity was partially filled with calcite cement (Table 5), and it was therefore not analytically replaced with material of granite density.

Table 6. Mass and volume values for 7 sandstone samples

Sample	mass wet (kg)	mass dry (kg)	volume of pore space (m^3)	% change	Total Volume (m^3)	Porosity	Reaction to dilute HCl
1	0.112	0.108	3.792E-06	5.6%	4.465E-05	8.5%	very reactive
2	0.121	0.118	3.663E-06	5.0%	4.811E-05	7.6%	very reactive
3	0.052	0.050	1.706E-06	5.5%	2.052E-05	8.3%	little reaction
4	0.041	0.040	9.560E-07	3.8%	1.620E-05	5.9%	very reactive
5	0.036	0.035	7.878E-07	3.6%	1.413E-05	5.6%	little reaction
6	0.312	0.302	1.040E-05	5.5%	1.242E-04	8.4%	moderate reaction
7	0.203	0.200	2.989E-06	2.4%	7.850E-05	3.8%	very reactive

Table 7. Average sandstone sample density and porosity and difference in density from granite.

average % change	average density (kg/m^3)	average porosity
4.5%	2531	6.9%

One estimate of the shear stress required to move a crest nuclear boulder is the theoretical "critical shear stress" $\tau_c = \tau_c^* g(\rho_s - \rho_w)d_i$, where τ_c^* is dimensionless critical shear, g is gravity, di is the intermediate axis of the boulder, and ρ_s and ρ_w are the densities of sediment and water respectively. The difference in

sediment density calculated here (Table 7) leads to a 7% decrease in critical shear, assuming typical values for the other variables. While it is clear that the lower density would lead to a higher probability of CNB mobility (Nicol et al., 2014), it is less certain that this magnitude of density difference is meaningful, given the high safety factor used in the design.

5.3.2 CNB Shape

As described in section 5.3.1, critical shear is proportional to τ_c^*, dimensionless critical shear. Dimensionless critical shear varies with environmental factors (besides the submerged weight of the particle and applied shear stress) that control the probability of particle motion. These environmental factors include hiding factor (Andrews 1983) and shape, which controls drag.

The CNBs were modeled for stability assuming they were spheres that initially moved by rotating forward over a 0.3 ft high fulcrum (Tetra Tech 2015). The presence of a fulcrum, imposed by downstream footer rocks, was not present in design drawings (Fig. 64), but may have been present in some of the berms (Fig 65). Therefore some CNB motion may have been from sliding rather than tipping.

The CNBs are actually blunt rectangular solids rather than spheres (Fig. 65), and thus have different drag coefficients. Drag coefficient is inversely proportional to τ_c^*, and will therefore influence the probability of motion. The typical drag coefficient for a sphere ranges from 0.2 to 0.47, whereas it is 1.07 for a rectangular solid (e.g., White 1976). The considerably higher drag on a blunt object compared to a sphere could lead to an underestimate of CNB mobility during modeling. However, Tetra Tech (2015) assumed a drag coefficient of 1.2, a very conservative value for either a sphere or blunt rectangle.

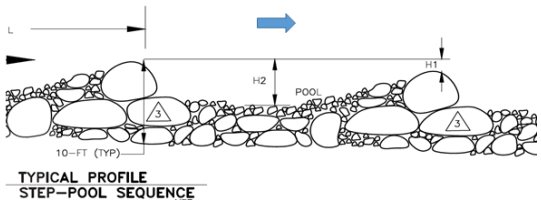

Figure 645. Longitudinal profile of typical step-pool. Design drawing of berms (from Tetra Tech 2015). Blue arrow indicates water flow direction.

Figure 656. Berms during construction.

5.3.3 Fluvial geomorphic relations for step-pool design

Tetra Tech (2015) showed that the geomorphic dimensionless ratios of the constructed step pools fall within the scatter of stable step pools published by Chartrand et al. (2011). It is unclear if this set of plots can discriminate unstable step-pool systems, given that the single unstable step-pool plotted by Chartrand et al. (2011) also plots near the cloud of stable channels (Fig. 17). Underscoring that point, we found that 3 out of 4 unstable checkdams we surveyed in Monterey fell within the scatter of stable channels as well (Fig. 66). However, the unstable checkdams generally plotted at the far end of the trend, away from the Carmel step-pool data.

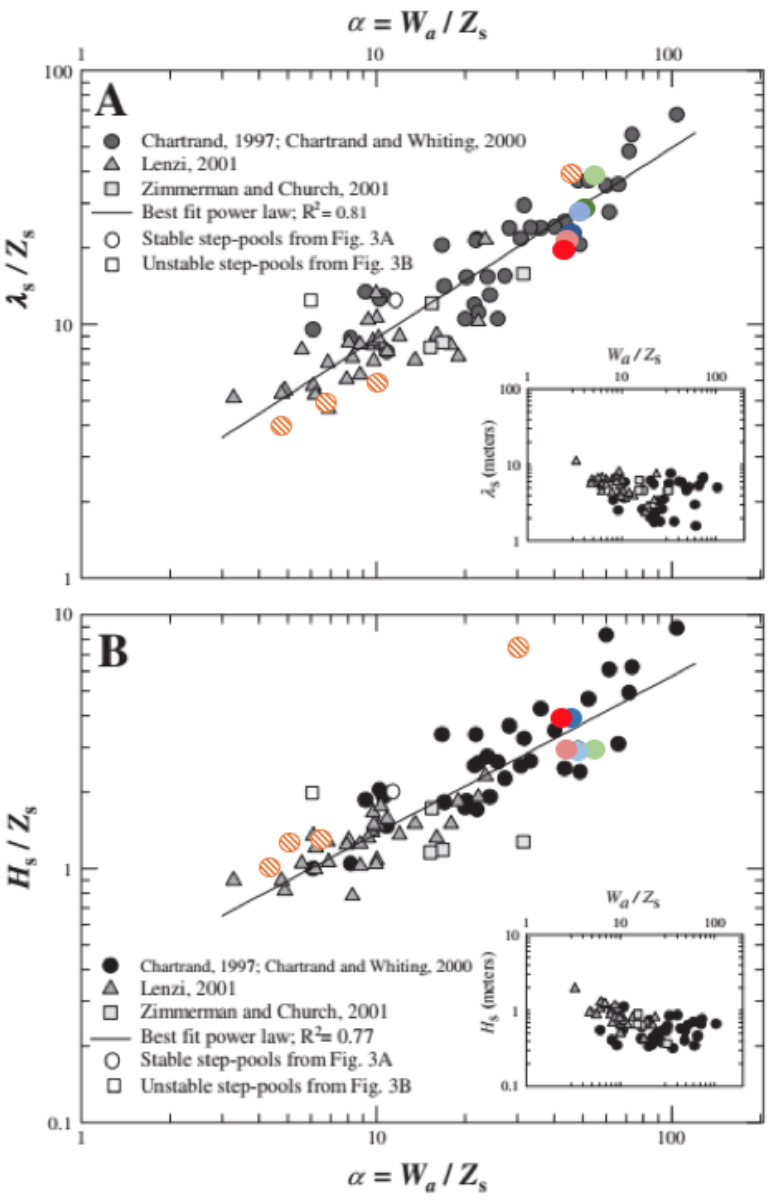

Legend		
Symbol	**Slope Range, Value**	**Data Source**
	Low, 2.3%	Design
	Low, 3.5%	Design
	Medium, 3.6%	Design
	Medium, 4.5%	Design
	High, 4.6%	Design
	High, 5.0%	Design
	N/A, >10%	Unstable checkdams

Figure 66. Plot of dimensionless ratios from natural step pool systems (figure modified from Chartrand et al. 2011). Plot includes step pools from CRRDR design (solid colored dots; Tetra Tech (2015)) differentiated by slope range. Unstable checkdams that we surveyed in Monterey are shown as striped dots. (A) Dimensionless pool length (λs/Zs) and (B) dimensionless step height (Hs/Zs), each as a function of the step-pool aspect ratio, or dimensionless width (Wa/Zs), where λs is the wavelength, Zs is the step drop height, Hs is the steph height, and Wa is the width of the active channel, see Figure 16 for definition of variables.

The ratio of pool-to-pool spacing to bankfull channel width as a function of slope can be compared to reference channels plotted by Rosgen (2006) (Fig. 67). The constructed Carmel step pools generally did not fit within the scatter

of reference channels plotted by Rosgen (2006). As the slope increased, the points came closer to the trend line, but it appears that either the pool-to-pool spacing was smaller or the channels were wider than the reference streams since all points were well below the scatter of stable channels (Fig. 67). The unstable Monterey check dams were too steep to plot directly on Figure 67, but would have been close to the model line if it were extrapolated far enough to the right.

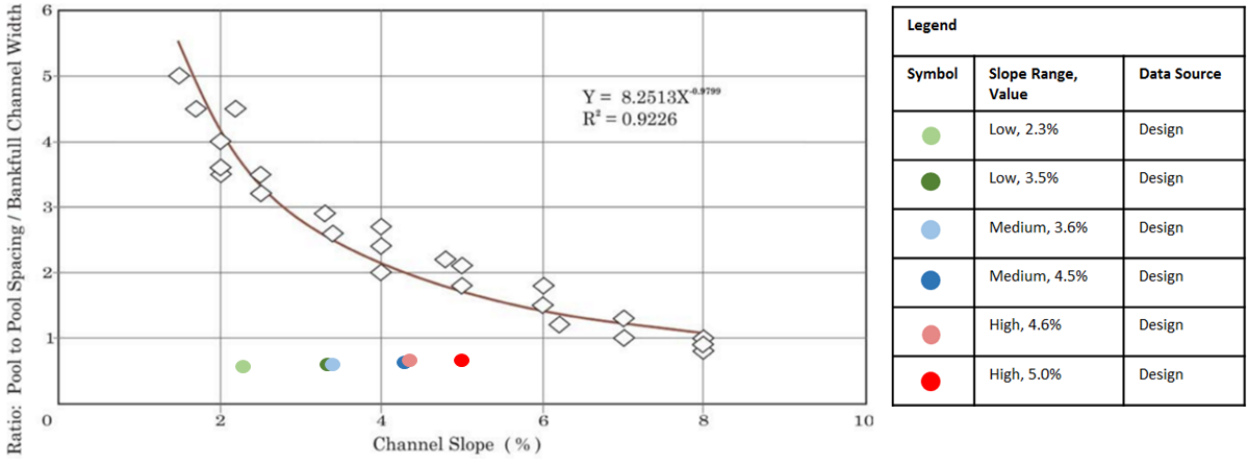

Figure 67. Ratio of pool-to-pool spacing to bankfull channel width as a function of channel slope (from Rosgen 2006). Colored dots are dimensions of step-pools in the project (Tetra Tech 2015), arranged by slope range.

Our assessment of the ability of Chartrand et. al (2011) and Rosgen (2006) plots to discriminate unstable step pool design may be flawed because the unstable check dams that we surveyed had a much higher average slope than that found in the constructed Carmel step pools. In summary, reference channels from Rosgen (2006), suggest that the Carmel pools were closely spaced, which could lead to higher shear stress against the CNBs and berm structures in high flow conditions.

5.4 Comparison of blueprint drawings to channel morphology in "reroute" reach

We compared the cross sectional geometry of the low-gradient reroute reach to blueprints, upstream reference reaches, and to stable channels of the broader region.

Figure 68 shows that the geometry of the reroute cross sections compared very well with the original constructed channels (assumed to be represented by blueprints) after one runoff season. Cross section 5 has an unresolved error erroneously showing a gross misalignment with blueprint data. Cross section 1 shows the erosion related to expanding the radius of curvature of near pool 12 (Fig. 56). Other minor differences between blueprints and cross sections probably indicate variability between the construction drawings and as built geometry.

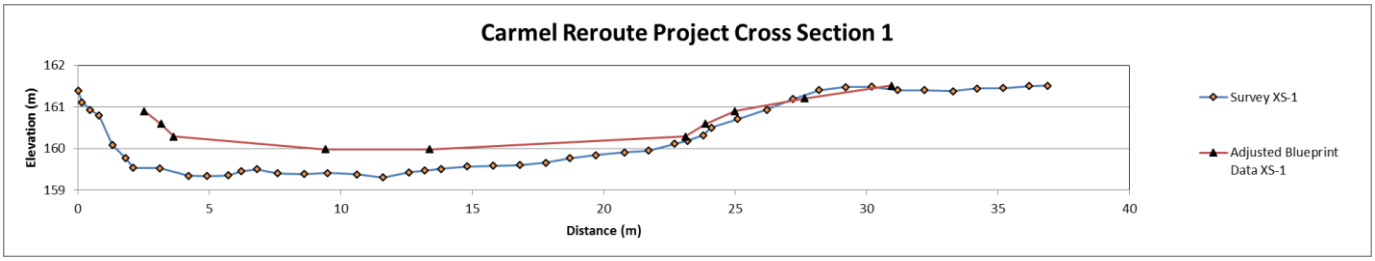

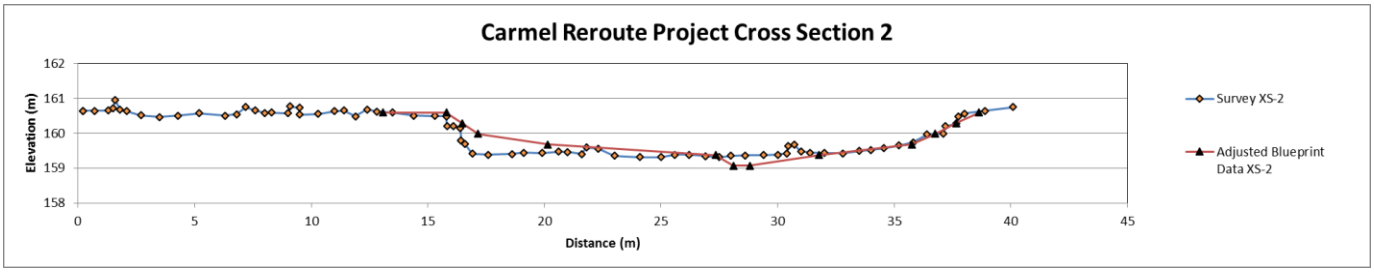

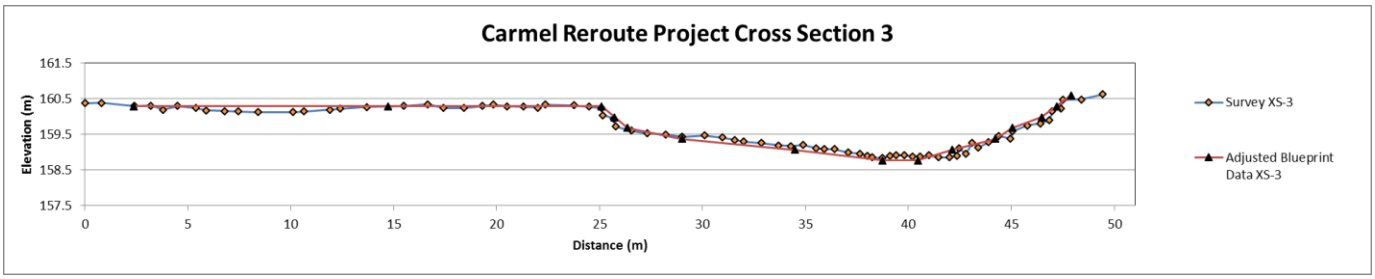

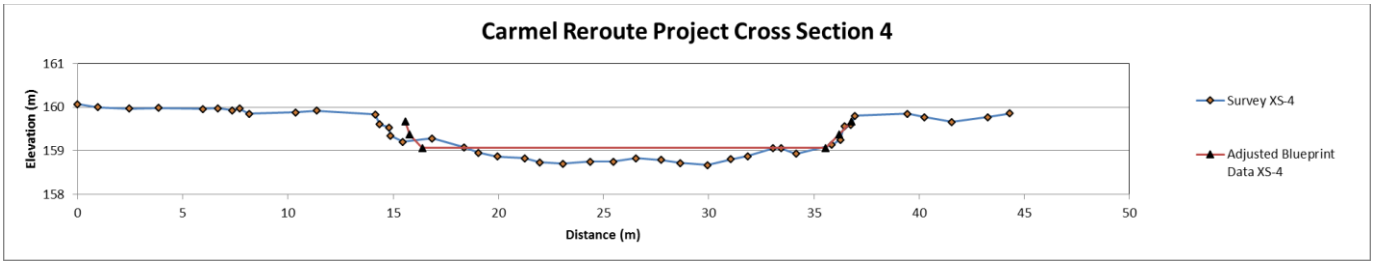

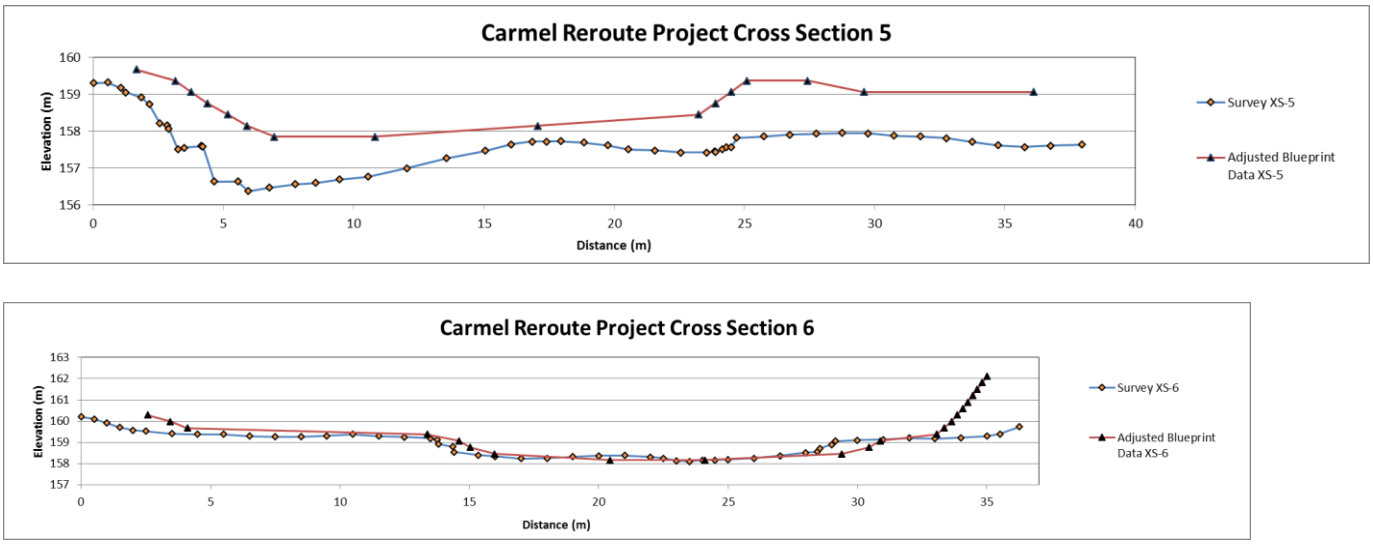

Figure 68. Six cross sections surveyed in the "reroute" reach of the CRRDR project (Fig. 20).

5.5 Comparison of channel morphology to regional reference channels

Channel cross sectional area is a function of drainage area (e.g., Dunne and Leopold 1978). To assess the size of the surveyed channels, we compared the cross sectional geometry of the surveyed cross sections and blueprint cross sections with reference cross sections measured upstream from the CRRDR project and with regional reference channels surveyed by Hecht et al. (2013). Table 8 compares the upstream reference channels (T1 to T6) to the reroute channels in terms of bankfull area, width and depth. The reference channels were surveyed upstream of the project (within 2 km of the project) before WY 2016 winter runoff began (Lee Harrison, NOAA/USGS unpublished data).

Table 8: Bankfull geometry of surveyed and blueprint channels. "RR" is from the reroute reach. "T" is from the upstream reference reach.

Transect	Area (ft^2)	Width (ft)	Depth (ft)	w/d
RR 2	231	73	3.2	23
RR 2 blueprint	238	75	3.2	24
RR 4	256	96	2.7	36
RR 4 blueprint	133	70	1.9	36
RR 6	128	51	2.5	20
RR 6 blueprint	127	53	2.4	22
T 1	172	71	2.4	51
T 2	347	89	3.9	23
T 3	165	48	3.6	14
T 6	127	53	2.4	22

We compared the bankfull area of the surveys and blueprints in Table 8 with broader regional streams in figure 69. All of the data plot on a trend with geomorphically stable streams from the region, especially those labeled "Inland South Bay and Monterey Bay." That subgroup includes two other reference sites in the Carmel watershed (Bluff Camp and Millers Fork). The general agreement between the reroute cross sections and the regional reference streams provides some confidence that the constructed stream reach will undergo only minor and slow adjustments through time, in keeping with the overarching project goals (Tetra Tech 2015). The step pool sections below the reroute reach provide very strong grade control, so the reach is protected from head cuts migrating up from the steeper downstream reaches. There remains a risk that uncontrolled evolution of the upper Carmel reach will negatively impact the reroute reach from above.

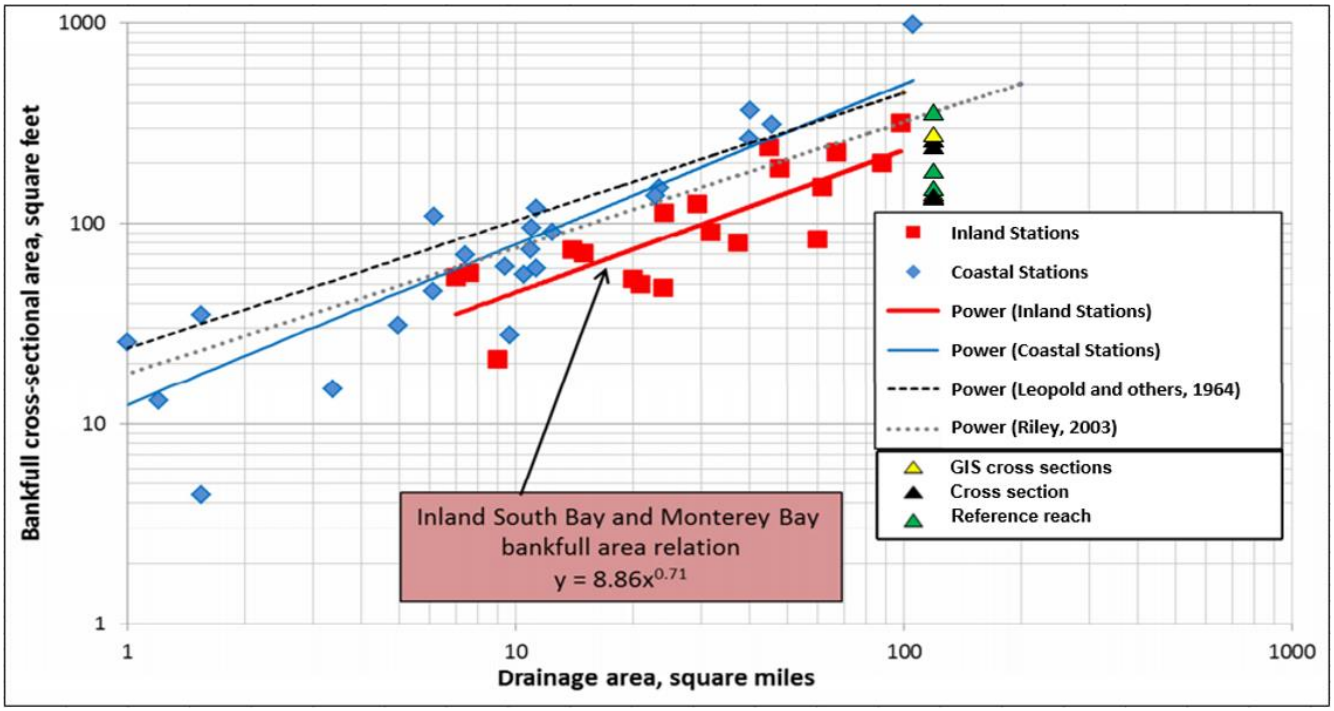

Figure 69. Cross sectional area from Table 8 plotted as a function of drainage area on regional curves of bankfull geometry (Modified from Hecht et al. 2013).

5.6 Comparison of channel substrate to local reference channels

Five significant point bars or side-attached bars formed during the first year of flow. Point bars form when sediment is deposited in areas of low velocity flow and reduced water depth along the inside of meander bends. The most downstream point bar, downstream of Pool 1, shifted the thalweg to the right bank and buried the pilot channel (Figs. 25 and 26). Likewise, the other four point bars have narrowed the adjacent channels and shifted the thalweg to the opposite side, accentuating the post-construction geometry.

We performed particle counts on four of the point bars, spanning the length of the project. The particle distribution graphs of the four surveyed point bars show poor sorting and remarkable uniformity along the length of the project (Fig. 70).

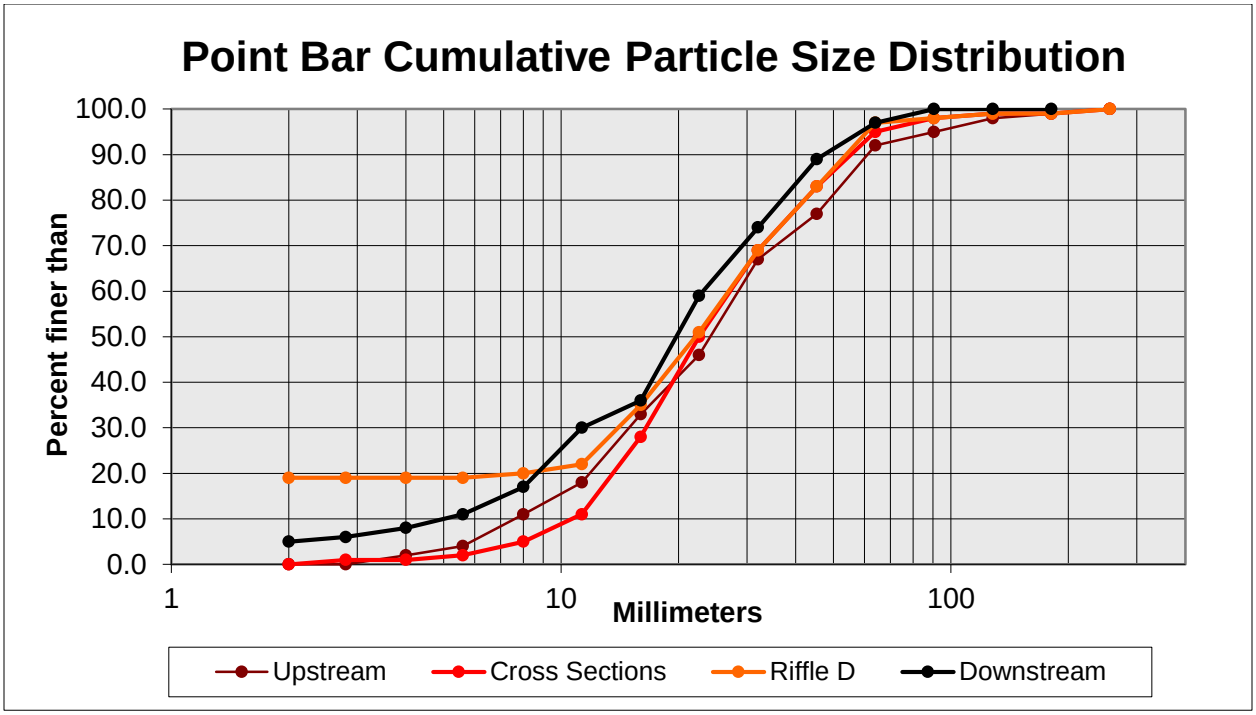

Figure 70. Cumulative frequency distribution of the four surveyed point bars.

The cumulative particle size distribution shows that the four point bars have equivalent particle size distributions except for the D16 diameter, which varied from 0 to 14 (Table 9). The graphical mean and 50th percentile (median) are greatest at the most upstream point bar and become finer downstream, although the magnitude of fining is insignificant.

Table 9. Particle size percentiles (D16, D50, D84) for point bar pebble counts.

Point Bars	D_{16} (mm)	D_{50} (mm)	D_{84} (mm)	Graphical Mean
Upstream	9.4	28	54	30
Cross sections	14	24	49	29
Riffle D	2	23	47	23
Downstream	8	20	40	23

The point bar particle size histogram is symmetric except for a large percentage of small, sand particles at the most downstream point bars (Fig. 71). The histogram shows that the modeof the downstream, cross section, and upstream point bars are coarse (22.6 mm) or very coarse gravel (32 mm). The point bar at riffle D is bimodal, with the major mode in the sand range.

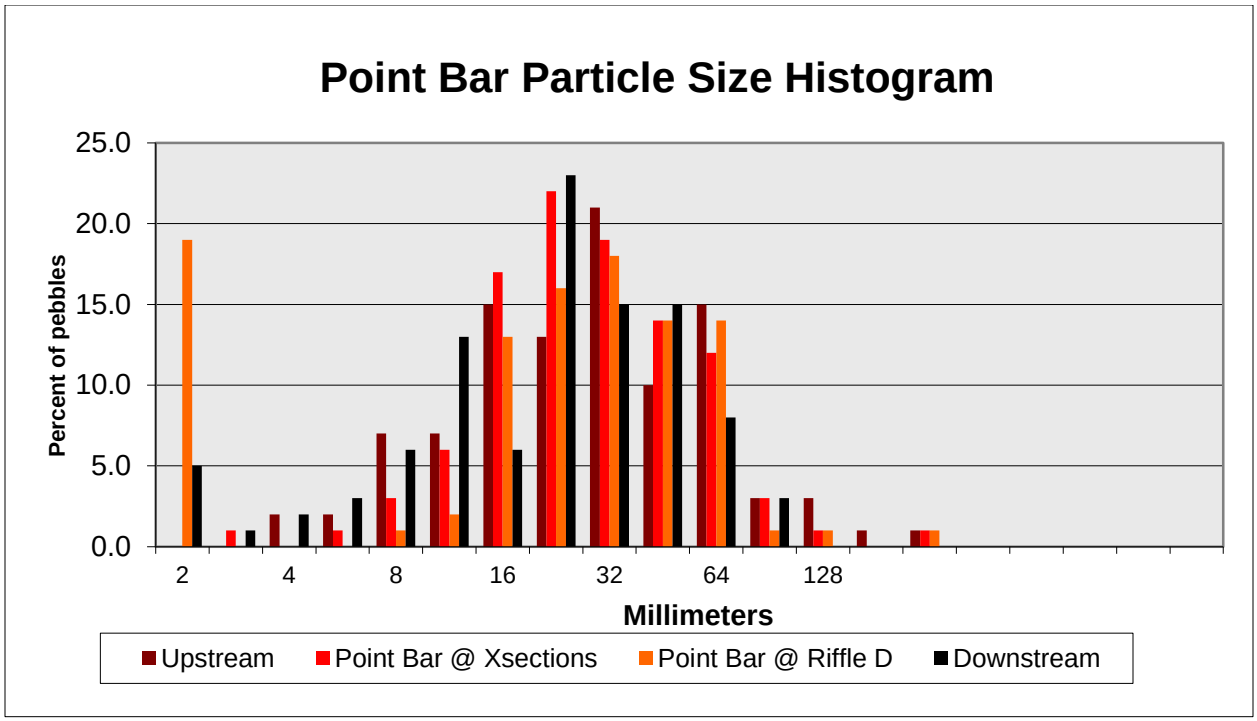

Figure 71. Histogram of point bar particle size frequency.

Particle counts were also conducted at surveyed cross sections of the river reroute (RR 1-6; Fig. 20). The RR pebble counts contained more scatter between cross sections than the point bars (Fig. 72).

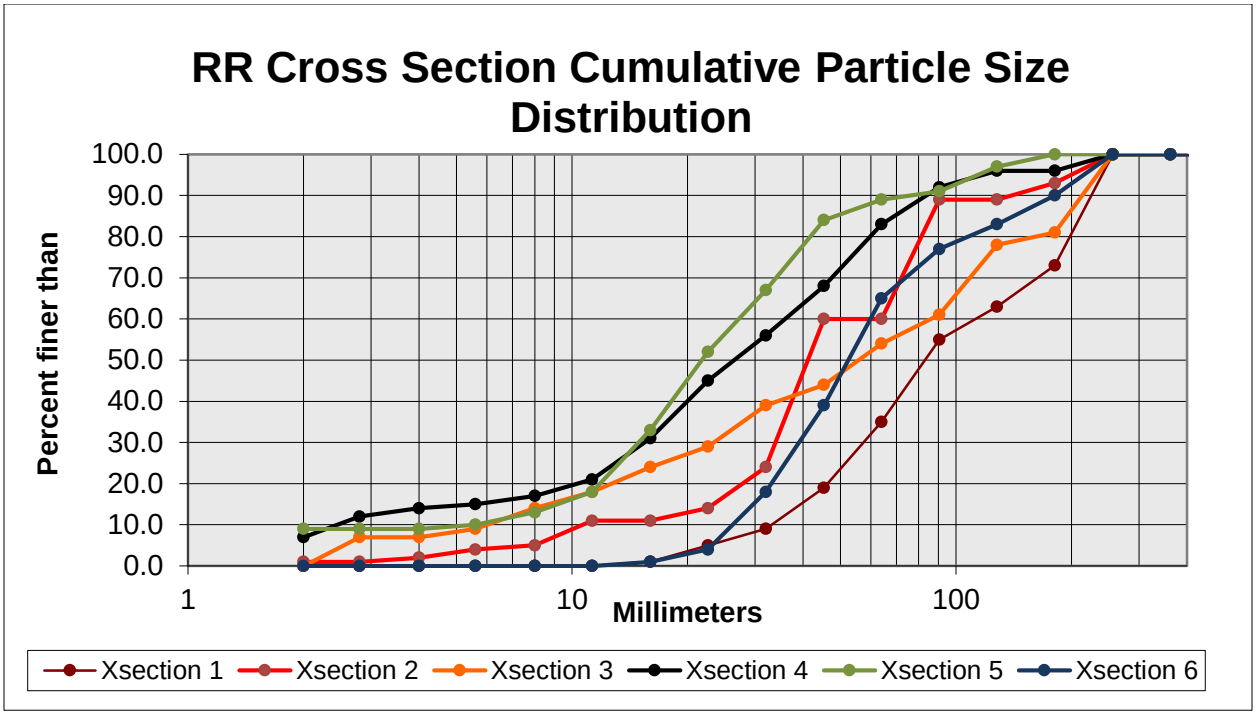

Figure 72. Cumulative particle size distribution of six RR cross sections.

Cross section 1, the most upstream cross section, contained the coarsest particles while cross section 4 had the most consistently fine particles. Compared to the point bars the cross sections consistently had larger, coarser particles, which is as expected, given the stronger flows within the channels. The histogram of the percent of pebbles per size class shows the same scatter of cross section particle sizes with a more negatively skewed distribution (Fig. 73).

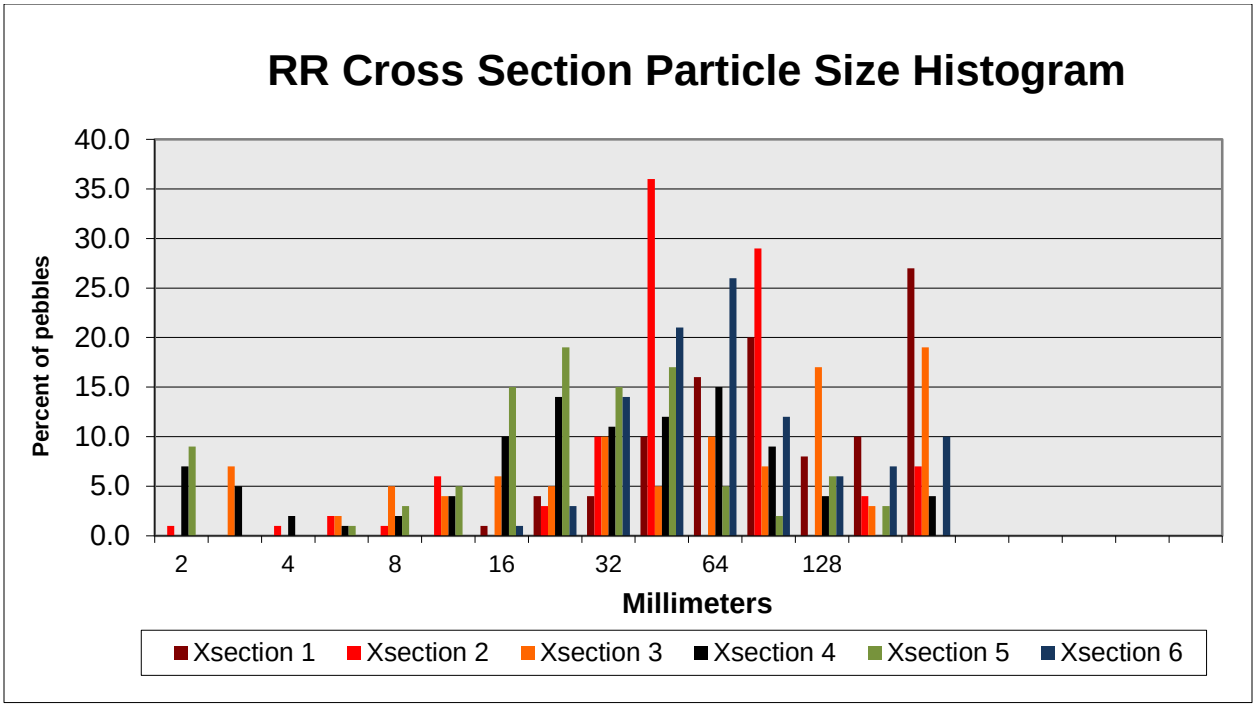

Figure 73. Histogram depicting the percentage of pebbles found in each particle size class for RR cross sections 1-6.

The average particle size was greatest at cross section 1 and decreased downstream until cross section 6, which had the second highest average particle size (Table 10).

Table 10. Particle size percentiles (D16, D50, D84) and graphical mean for RR cross section pebble counts.

RR Cross Section	D_{16} (mm)	D_{50} (mm)	D_{84} (mm)	Graphical Mean
1	42	83	220	115
2	25	42	84	50
3	10	58	190	86
4	5.9	27	69	34
5	10	22	44	25
6	30	50	150	77

Before winter runoff, particle counts were measured on six reference cross sections upstream of the reroute channel (T1 – T6). The pebble counts at these cross sections were completed after 5 years of drought and contained significantly finer sediments/sand than the particle counts completed for this study (Fig. 74). There was significant scatter in particle size distributions

between the reference cross sections (Fig. 74), similar to the scatter from the study cross sections, but exhibiting a wider range of fines between sections.

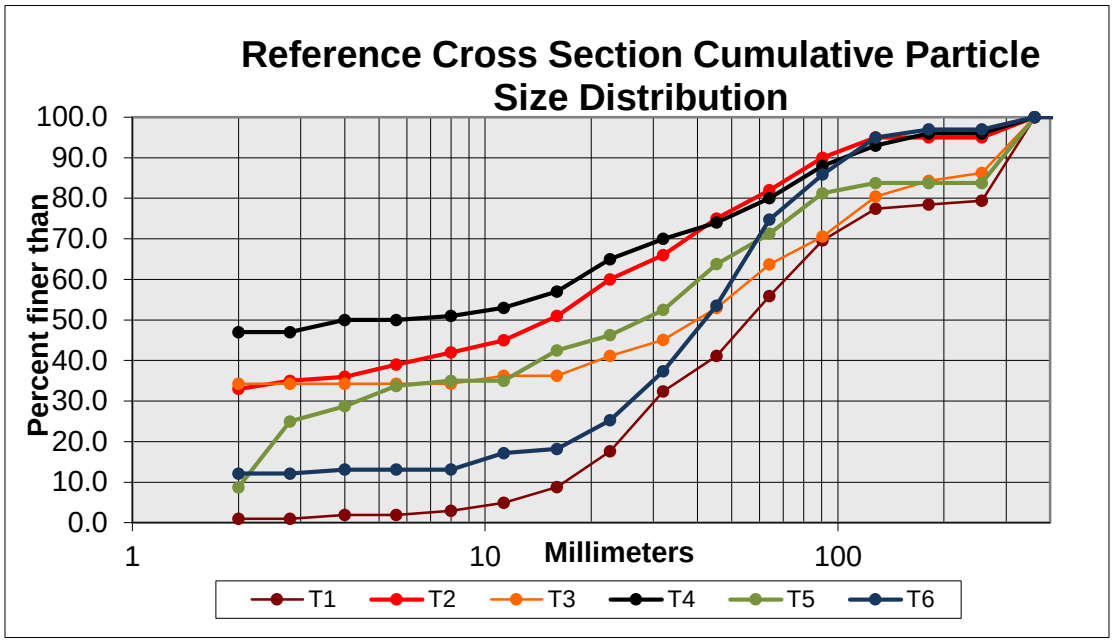

Figure 74. Cumulative particle size distribution of reference cross sections.

The histogram of the reference cross sections also shows the large quantity of fine sediment present (Fig. 75), as well as the significant proportion of small boulders (256 mm). The mode of cross sections T2, T3, and T4 fell under <2 mm, or sand particle size. Cross section T5 was bimodal with 13 particles at 2 mm and 13 at 256 mm, showing an array of particle size classes present.

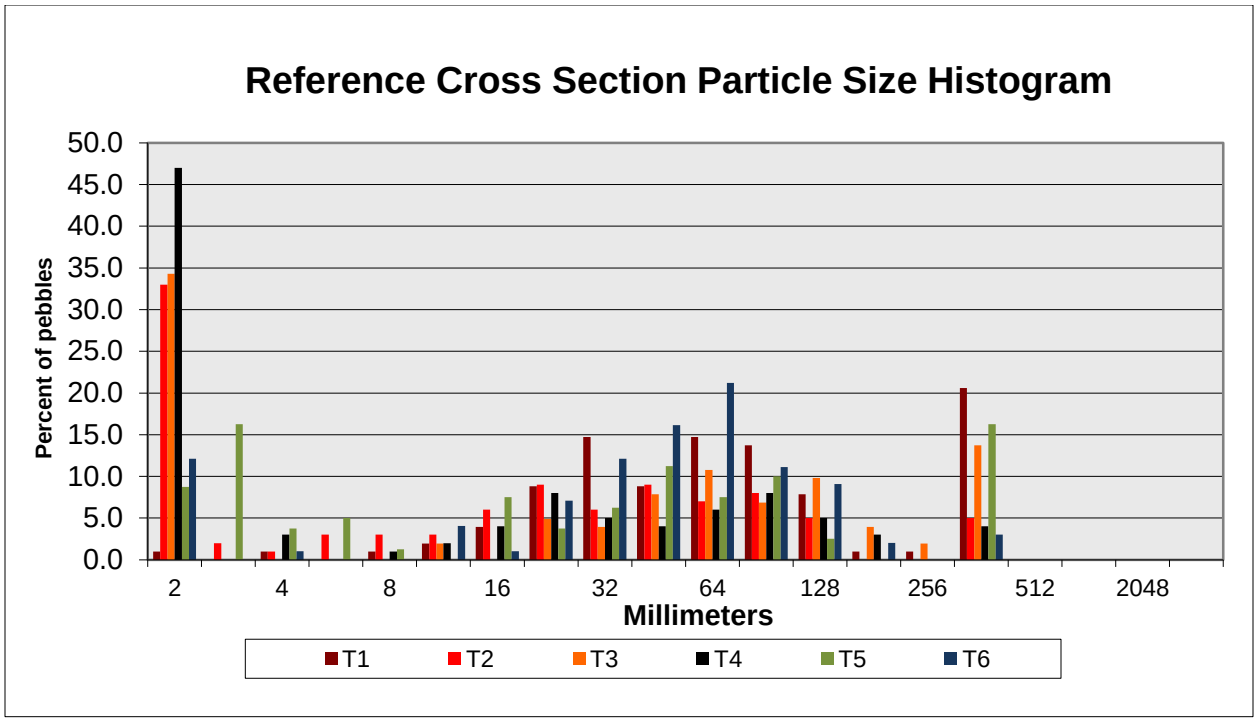

Figure 75. Histogram of reference cross section particle size frequency.

The median (D50) particle size of reference cross sections T1–T6 did not follow a particular pattern from the most upstream (T1) to the most downstream (T6) and ranged from 3.5 mm to 59 mm. Cross sections T2 and T4 consisted of a majority of fine, sand sediments, and had a D84 of 70 mm, much lower than the 84th percentiles of the other surveys (Table 11).

Table 11. Particle size percentiles (D16, D50, D84) and graphical mean of reference cross section pebble counts.

Reference Cross Section	D_{16} (mm)	D_{50} (mm)	D_{84} (mm)	Graphical Mean
T1	22	59	280	120
T2	2	59	70	43
T3	2	40	190	77
T4	2	3.5	70	25
T5	2.4	30	290	107
T6	10.1	43	90	48

Particle sizes for the point bars, RR cross sections, and reference cross sections were averaged, respectively, and then compared using a cumulative particle size distribution and histogram. The reference cross section (T in Fig. 15) has

significantly more fines than either the study cross sections or the point bars. The Point bars were finer and better sorted than both the RR cross sections and reference cross sections (Fig. 76).

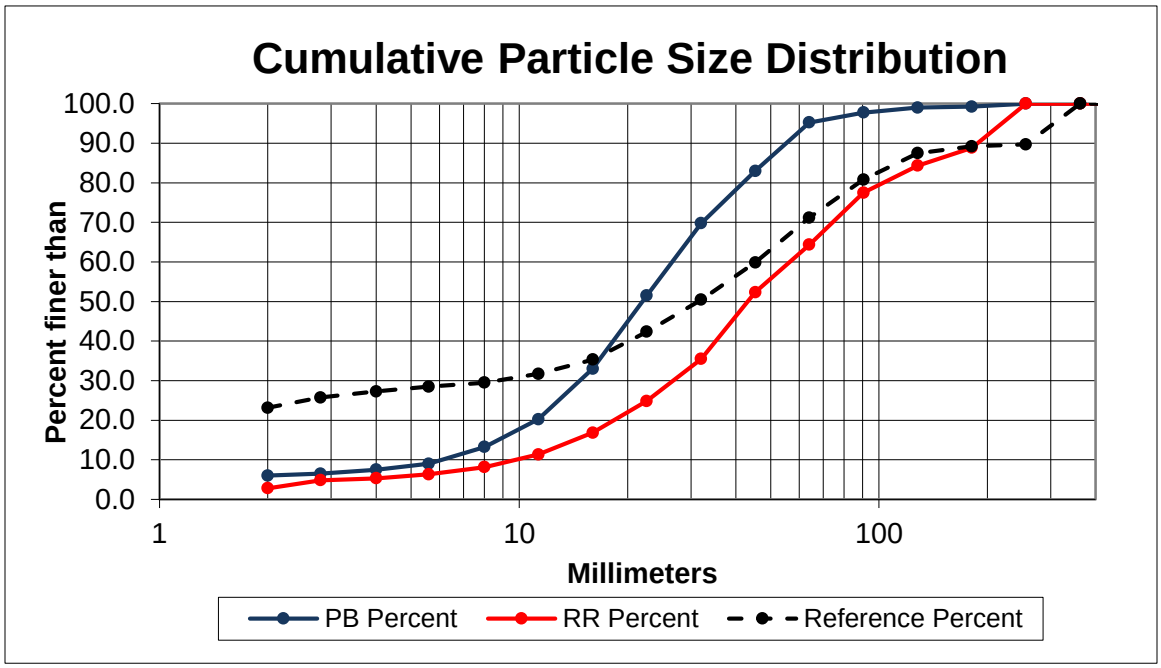

Figure 76. Cumulative particle size distribution of average point bar, our cross section and upstream cross section pebble counts.

The greater amount of fines in the reference cross sections compared to the study cross sections might have been because the reference measurements were made late in the season, after fines had dropped from waning flows. To test that idea, we synthetically added fines to the study cross section data, to match the fines in the reference reaches. The cumulative percentage of <2 mm particles from reference cross sections was replicated in RR cross sections. The remaining class sizes were then reduced proportionally to maintain the same particle total for the data set. The increase of fine, sand sediment to the RR cross sections shifted the distribution to closely follow the distribution of the reference cross sections (Fig. 77).

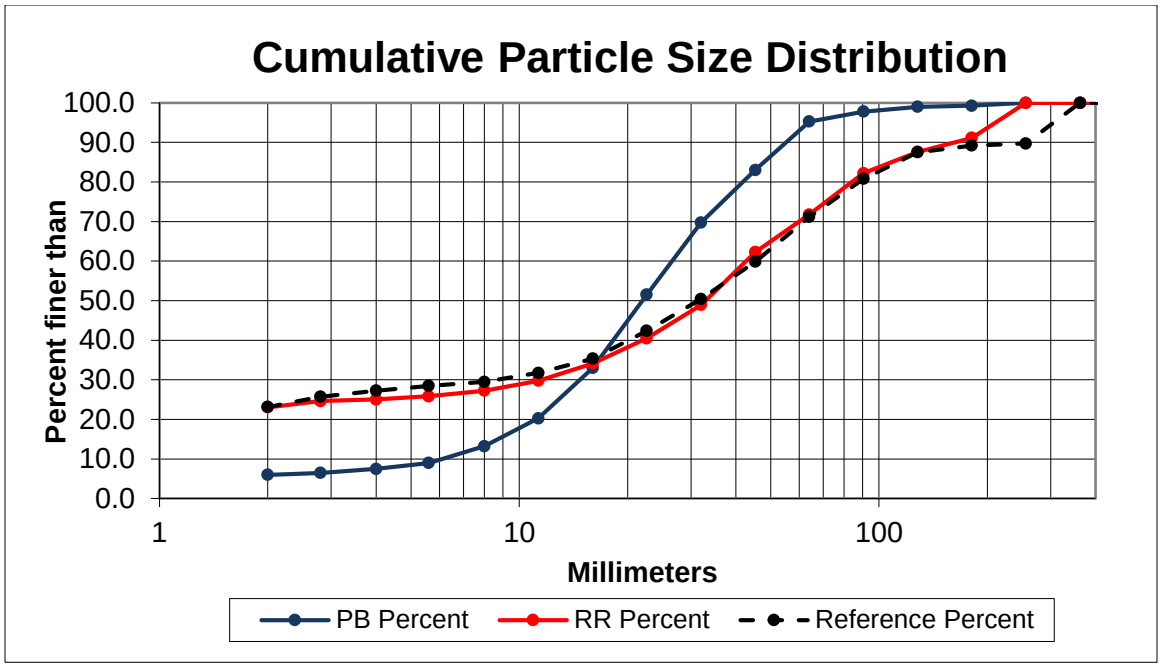

Figure 77. Revised cross section cumulative particle size distribution. Cross section became finer and follows upstream cross section distribution.

Particle diameters of the 16th, 50th and 84th percentiles were calculated for the average point bar, RR and reference cross sections. Table 12 shows that the upstream, reference cross sections had a particle size at which 16% of the material was much smaller than the point bar and RR cross section averages. This is due to the large quantity of fine sediments present in the upstream reaches. Particle size percentiles and graphical mean were also calculated for the revised RR cross sections, which included an equivalent amount of fine sediments as the reference site. Those values, included in parentheses in Table 12, are almost identical to the corresponding values at the reference site.

Table 12. Particle size percentiles (D16, D50, D84) and graphical mean of average point bar, RR cross section, and reference cross section pebble counts. The values in parentheses indicate the adjusted RR particle size percentiles with the added fine sediments.

Average	D_{16} (mm)	D_{50} (mm)	D_{84} (mm)	Graphical Mean
Point Bars	9.5	23	46	26
Reference	2	31	110	47
RR	16 (2)	43 (33)	140 (110)	66 (48)

5.7 Comparison of channel morphology to general reference channels

To further assess the reroute section we compared the geomorphology of the surveyed cross sections to general reference rivers plotted by Leopold et al. (1964; Fig 14). Measurements from the design blueprints indicate that the meander length of the reroute reach is approximately 640 ft (Fig. 78). The surveyed riffle cross section widths in that reach averaged 73 ft and the blueprint channel widths averaged 66 ft (Table 8). The surveyed and blueprint values compare well with other general natural rivers of the world (Fig. 79).

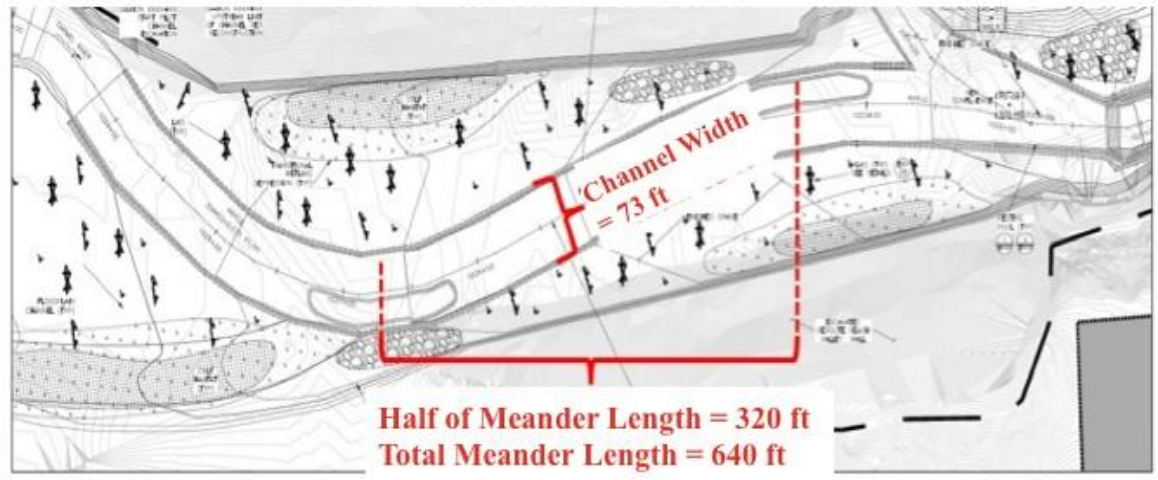

Figure 78. Design blueprints for Reroute reach (modified from Tetra Tech 2015). Average riffle width from current study.

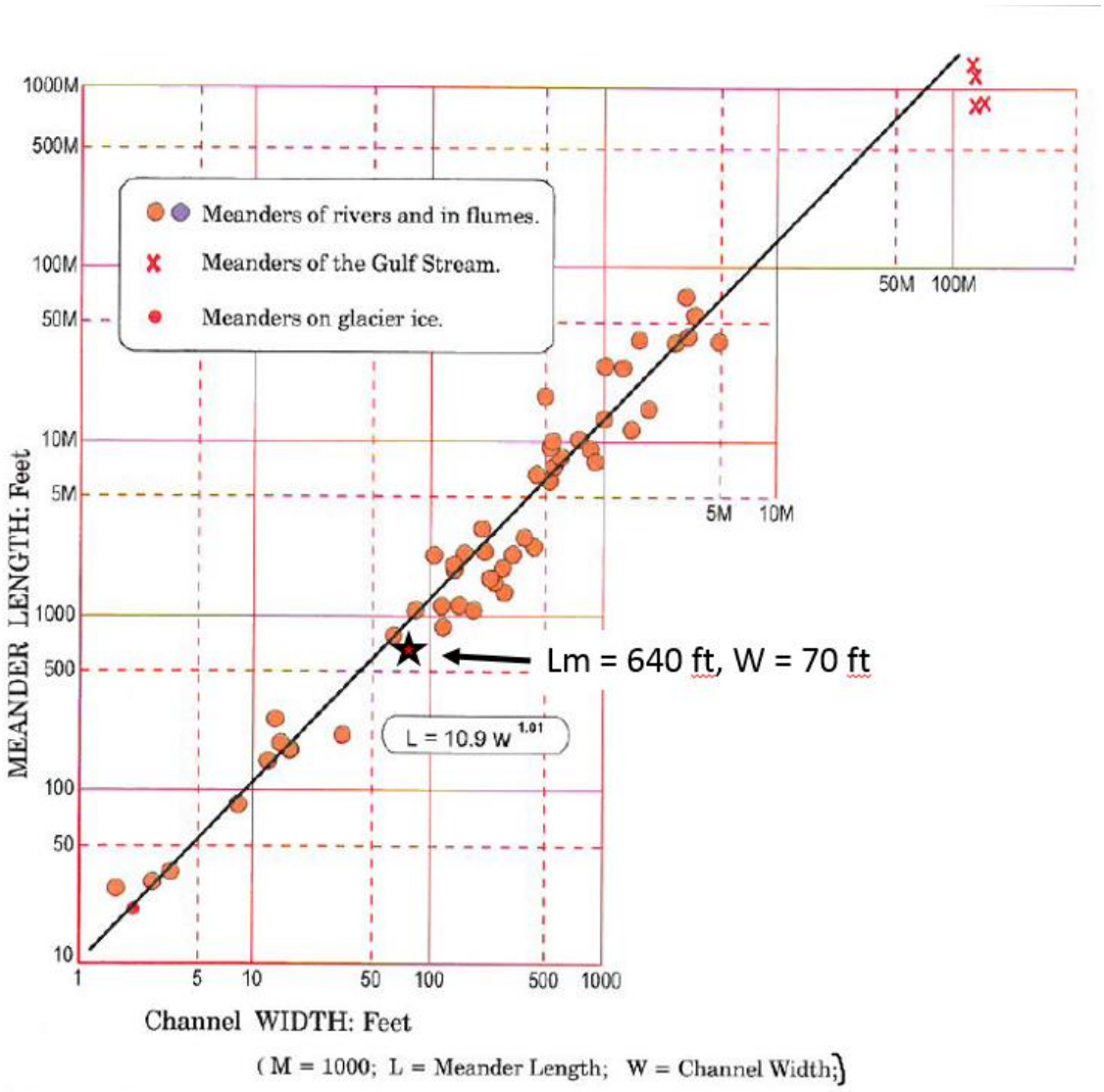

Figure 79. Relationship between meander length and channel width from Granite Construction blueprints graphed on published natural stream relationship graph. (Graph modified from: Rosgen, 1996; Original relationship from Leopold et al. (1964))

The radius of curvature to bankfull width ratio (Rc/Wbkf) plays an important role in the risk of stream bank erosion. In general, a lower ratio indicates a tighter bend, and corresponding higher risk of excess bank erosion.

We examined the Rc/Wbkf ratios of the bends in the project and found the highest ratio to be 3.4 and the lowest ratio to be 0.8 (Fig. 80; Table 13). We found that the curves with reasonably high Rc/Wbkf ratios experienced less change than those with small ratios, as predicted from Figure 81. In some

areas, the pattern design of the channel was controlled and restricted by existing valley conditions, but some of the bends were in areas that did not seem to have any placement constraints (Table 13).

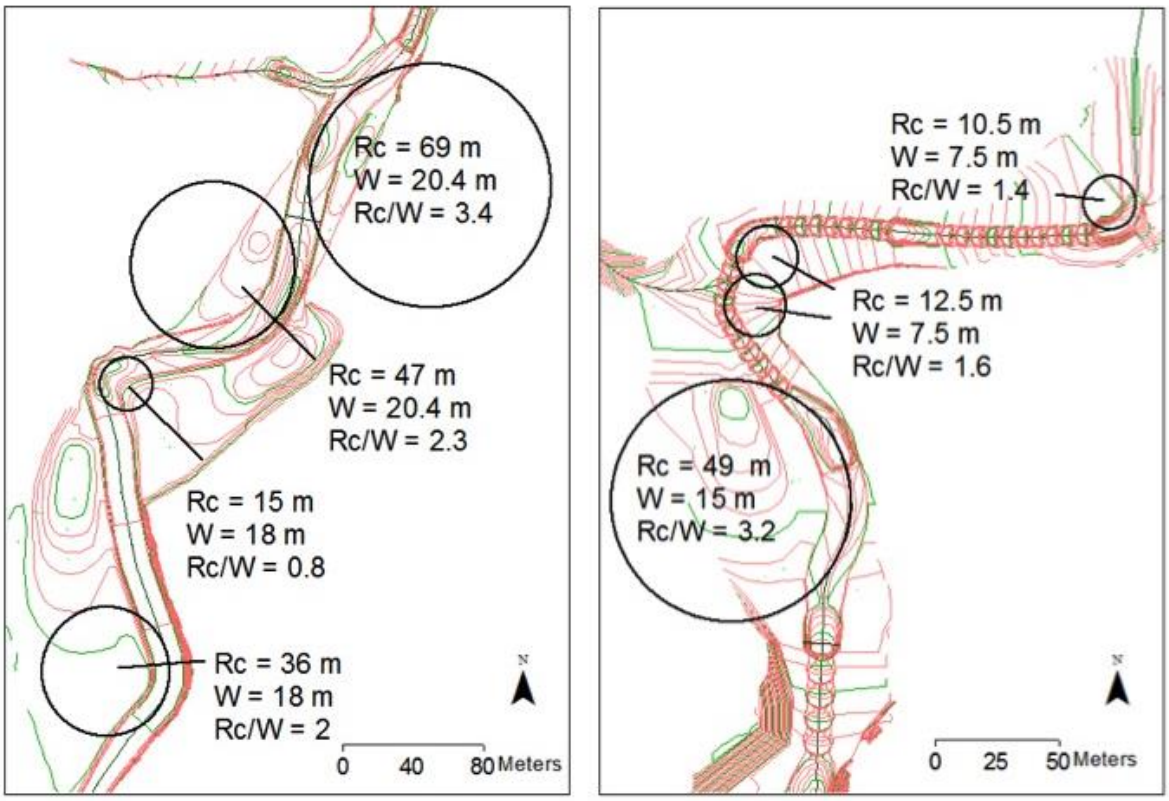

Figure 80. R_c/W_{bkf} ratios of Carmel River Reroute Project. Left map includes the upper Carmel reach (bottom), pool 12, and the reroute reach. Right map includes Riffle D, pool 4, berm sections A through C and pool 1 (top of map). Table 13 summarizes the data.

Table 13. R_c/W_{bkf} ratios, Rosgen's near bank stress (NBS) rating (Rosgen 2006), consequences, and context. The bends with higher R_c/W_{bkf} ratios experiences less change than those with lower R_c/W_{bkf} ratios.

Location	Rc/Wbkf	NBS rating from Rosgen Table	Consequence	Context
Downstream of Pool 1	1.4	Extreme	Right bank completely eroded	Pattern controlled by existing valley conditions
Pool 3 and Section C	1.6	Very High	Large lateral failure around step pools	Pattern controlled by existing valley conditions
Pool 4 and Riffle D	3.2	Very Low	None	No constraints
Upstream of Section H – Pool 9, Riffle I, and Pool 10	3.4	Very Low	None	No constraints
Pool 11 and Riffle K	2.3	Low	None	No constraints
Pool 12 and Upper Carmel Reach	0.8	Extreme	Significant erosion of left bank	River had to follow bedrock wall on Pool 12
Upper Carmel Reach – beginning of constructed	2	High	Apex of bend moved tens of meters	No constraints

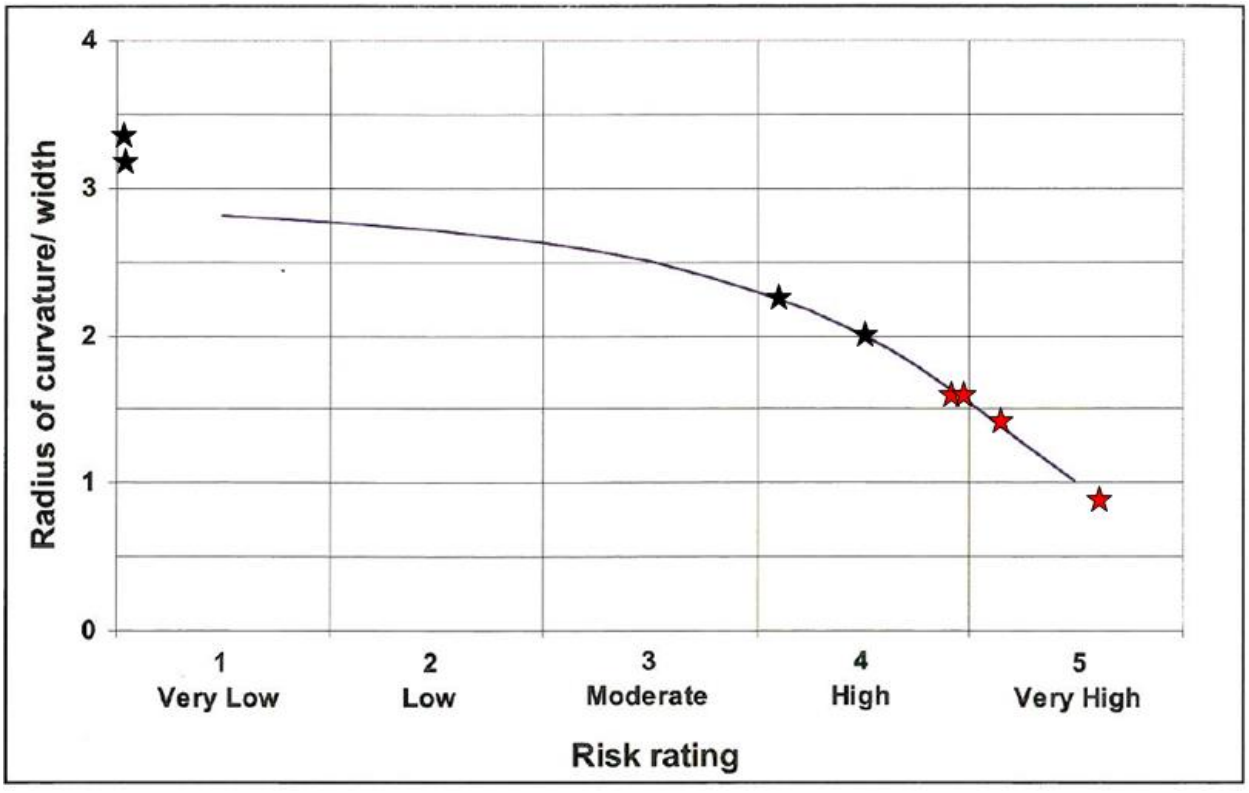

Figure 81. The risk of stream bank erosion based on the Rc/Wbkf ratio. (figure modified from Rosgen (2006)). Red stars indicate bends in the CRRDR project where outer bank erosion was present. Black stars indicate bends in the project where bank erosion was not evident. See Figure 80 and Table 13.

6 Discussion

The main goals of our project were to assess the first year adjustments of the Carmel River Reroute Project, compare the reroute channel to natural stream channels in order to determine why some of those adjustments may have occurred, and establish the baseline for long-term monitoring of the restoration project. While most of the project remained in excellent condition following the first year, several issues came to light. Our visual assessment showed that there were moderate to significant impacts in the upper Carmel River reach and in sporadic parts of the combined flow reach, but the reroute Channel remained stable. Figure 82 summarizes the areas where the project has experienced moderate and more significant changes during the first year of flow.

The Upper Carmel River Reach was constructed with a pilot channel with cohesionless banks and no bank protection, so changes were expected. However, the large amount of bank erosion (Figs. 56 and 60) required the rest of the system to process that bank-sourced sediment load in addition to the load entering the site from upstream. Since river stability is inherently tied to sediment load, excess sediment can adversely stress the rest of the project downstream. The extra sediment likely fostered the rapid growth of several new point bars in the project. The excess bedload could also eventually cause the infilling of the resting pools and step-pools, which would impair low flow steelhead migration. In addition, the lack of bank strength and high bed load could potentially lead to stream braiding in the Upper Carmel reach, also impairing low flow steelhead migration.

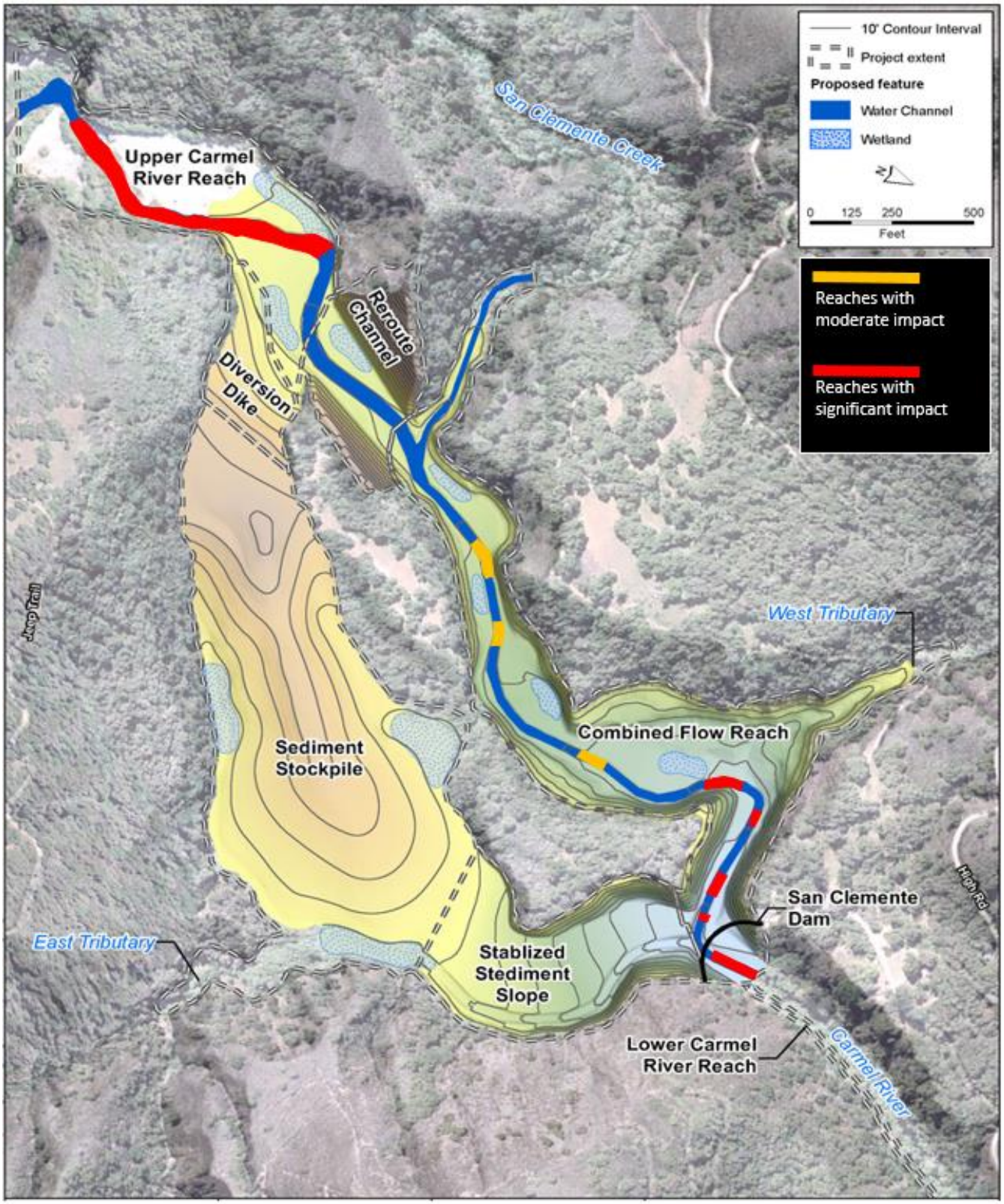

Figure 82. Summary of geomorphic change magnitude along the constructed channel. Basemap modified from URS (2012).

In the Combined Flow Reach, step-pool sections E, G, and H experienced moderate changes (e.g., Figs. 48 and 49). Although only four CNBs moved in these sections, the movement of one CNB could cause other CNBs to become unstable. We saw the greatest change in step-pool sections A, B and C (Fig 82). Many of the berms in this section lost one or two CNBs (e.g., Fig 32). A great deal of structural strength of the berms comes from the "arch" shape that turns downstream-directed shear stress into side-directed compression against the banks. Therefore, the future stability of the structures may be jeopardized by the loss of one or more CNBs. Indeed, CNB loss may have been initiated in some cases by bank erosion that loosened the edge of the arch structure.

The left floodplain by pool 4 and section C was significantly altered by deposition and local erosion (Fig. 83). During a high flow event, a nascent avulsion channel formed on the floodplain. If that channel were to grow and carry the main flow during low flow conditions, then almost all of the step-pools in section C would be bypassed. In the upper part of section B, the left bank was eroded to the bedrock, causing the water to partially bypass the step-pool design in both low and high flows (Figs. 30 and 31). This lateral failure could lead to the destabilization of a subset of the berms in Section B. However, the bend is adjacent to a bedrock wall, so future adjustment might be limited, and fish passage is not jeopardized at this time. The main impact in section A is that the most downstream berm (A1) is missing (figs 27 and 28). Berm A1 set the local base level for the project as a whole. The incremental effect of CNB or berm loss is to have a taller step on the next berm upstream, making fish passage incrementally more challenging, however, the step at A2 did not appear to be significantly higher than others in the section.

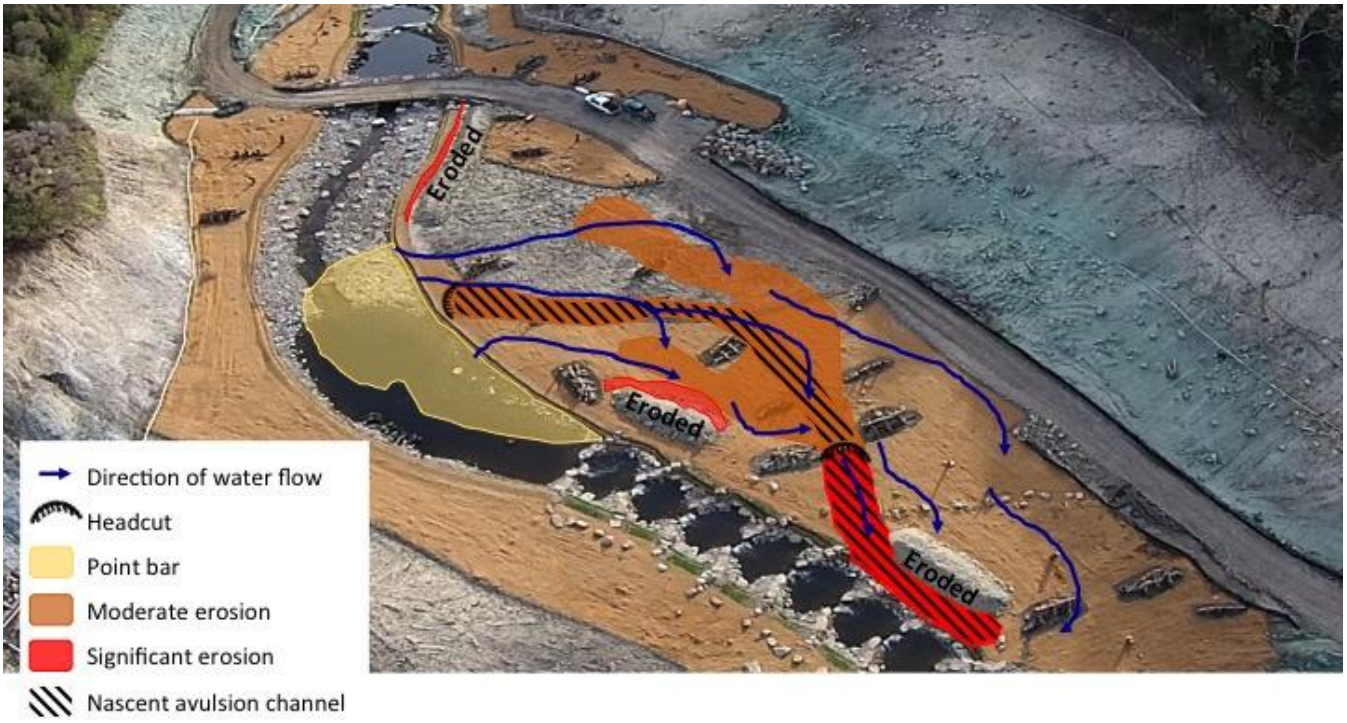

Figure 83. Detailed map of left floodplain adjacent to pool 4 and section C. Floodwater flow paths were determined from debris alignment on tree stems.

While the changes that occurred do not significantly impede mature fish passage, the geomorphic adjustments seen in the restoration project occurred prematurely, according to design goals (Table 1). During the study period the peak flows had recurrence intervals of 0.8 and 1.4 years (partial duration series). These flows resulted in CNB movement and bank erosion that do not meet the design goals set forth by Tetra Tech (2015; Table 1). While there was local impairment of the LWD structures, they did not fail from directly applied hydraulic stresses, they failed from lateral erosion of unstable banks.

Although we cannot definitively say why changes occurred prematurely, slope, tight radius of curvatures, or CNB modeling are just a few of the potential contributing factors. We found that the pool-to-pool spacing in the combined flow reach was generally lower than recommended by Rosgen (2006), but did conform to dimensionless ratios of Chartrand et al. (2011) (Figs. 66 and 67). In addition, we found a significant correlation between channel slope and bank condition. We saw more channel erosion in steeper channel reaches (Figs. 62 and 63). We found that bends in the river with reasonably high R_c/W_{bkf} ratios

experienced less change than those with small ratios (Fig. 81), as predicted by the Rosgen (2006) risk rating model. In the CNB stability calculations, the density for granite was used, but in actuality, sandstone was used for the CNBs. We found that the density of the sandstone used for CNBs is 5% less than granite, which propagates a 7% decrease in calculated critical shear. In addition, in the CNB stability modeling, a fulcrum was assumed to force CNB rotation at the point of incipient motion, however, a fulcrum was not clear in the blueprints, and was not always obvious in the constructed channel. The amount of shear stress required for the CNBs to slide off of their platforms was not taken into consideration.

The bankfull cross sectional geometry in the reroute reach conforms well with the blueprints, local reference channels, regional stable channels, and more general channels of the world (Figs. 68, 69 and 79), suggesting that the reach will not likely destabilize, unless forced from upstream changes.

With the baseline data from this report, the restoration project can be monitored for many years and the reasons of change may become clearer through time. When we compared our benchmarked cross-sectional surveys to the blueprints, almost every cross section followed the blueprints very closely. In years to come, we can superimpose new data onto our baseline data to see how the channel evolves over time.

In addition, continued collection of particle count data will allow us to see the effects and sources of added sediments to the system. Our initial particle count data for surveyed point bars, reroute channel cross-sections and reference cross sections indicate the sediment distribution of the reroute channel is behaving as expected. The reroute channel is successfully transporting sediment as evidenced by the formation of point bars throughout the system. This transported sediment may be sourced from the natural channel upstream of the reroute, or from the engineered streambed material (ESM) added during construction of the reroute channel. This indiscernible difference between particle sources shows that appropriately sized ESM was used for the project. Natural alluvial deposits of the San Clemente Creek Valley were characterized for the project by digging and sieving 6 test pits. The deposits were highly

consolidated and contained a median particle diameter (D_{50}) between 1.9 mm and 200 mm (Tetra Tech 2015). The average D_{50} particle size for the test pit samples was 40 mm, which is similar to the average reroute channel cross section median particle size of 43 mm (Appendix B).

In summary, the main goal of the restoration project was to create and maintain fish passage, with a focus on steelhead migration. This overarching goal was met following the first winter season. Fish passage might be at risk in the future if the lack of bank strength and high bed load leads to stream braiding in the upper Carmel reach, or if a new channel in the floodplain next to Section C grows and pirates the flow.

The overall impact of the new approach to dam removal has been far less than traditional catastrophic dam removal strategies and is sure to be a great example for future dam removal projects.

7 References

Andrews, E. 1983. “Entrainment of Gravel from Naturally Sorted Riverbed Material.” Geological Society of America Bulletin 94 (10): 1225. doi:10.1130/0016-7606(1983)94<1225:EOGFNS>2.0.CO;2.

Beck E., Geisler E., Gehrke M., Goodmansen A., Leiker S., Phillips S., Rhodes J., Schat A., Snyder A., Teaby A., Urness J., Wright D., and Smith,D. 2013. A Survey of Large Wood on the Carmel River: Implications for Bridge Safety Following San Clemente Dam Removal: The Watershed Institute, California State Monterey Bay, Publication No. WI-2013-04, 46 pp.

Bernhardt, E.., Sudduth, E., Palmer, M., Allan, J., Meyer, J., Alexander, G., Follastad-Shah, J., Hassett, B., Jenkinson, R., Lave, R., Rumps, J. and Pagano, L. (2007), Restoring Rivers One Reach at a Time: Results from a Survey of U.S. River Restoration Practitioners. Restoration Ecology, 15: 482–493. doi: 10.1111/j.1526-100X.2007.00244.x

Boughton D., East A., Hampston L., Kiernan J., Leiker S., Mantua N., Nicol C., Smith D., Urquhart K., Williams T., Harrison L. 2016. Removing a dam and re-routing a river: Will expected benefits for steelhead materalize in Carmel River, California? NOAA Technical Memorandum, NOAA-TM-NMFS-SWFSC-553. US Department of Commerce. Southwest Fisheries Science Center, Santa Cruz, CA. 89 pp.

Chartrand S., Jellinek M., Whiting P., Stamm J. 2011. Geometric scaling of step-pools in mountain streams: observation and implications. Geomorpholgy (129):141-151.

Chow K., Luna L., Delforge A. and Smith D. 2016. 2015 Pre-San Clemente Dam Removal Morphological Monitoring of the Carmel River Channel in Monterey County, California. The Watershed Institute, California State University Monterey Bay, Publication No. WI-2016-01, 50 pp.

Dunne, T., Leopold, L. 1978. Water in Environmental Planning. WH Freeman and Company, New York. 818 pp.

Endreny, T. and Soulman, S. 2011. “Hydraulic Analysis of River Training Cross-Vanes as Part of Post-Restoration Monitoring.” Hydrology and Earth System Sciences 15 (7): 2119–26.

Harrelson, C., Rawlins, C., and Potyondy, J. 1994. “Stream Channel Reference Sites: An Illustrated Guide to Field Technique.”

Hecht, B., Senter, A., Strudley, M, and Xu, L. 2013, New bankfull geometry relations for inland South Bay and Monterey Bay, Central California: Poster presented at 2013 State of the Estuary Conference, Oakland, CA.

Howard, A.D., 1982. Equilibrium and Time scales in Geomorphology: Application to sand-bed alluvial streams: Earth Surface Processes and Landforms, V. 7. p.303-325.

James, G. 2009. Carmel river basin- surface water resources data report water years 2004-2008. [Internet]. [cited 2016] Available from: http://www2.mpwmd.net/wrd/crbreports/WY%202004-08.pdf

Tetra Tech. 2015. Initial design report for channel restoration design for the Carmel River reroute and San Clemente Dam removal (CRRDR) project. 87 pp.

Leopold, L., and Bull, W. 1979. Base level, aggradation, and grade. Am. Philos. Soc. Proc. (23): 168-202.

Leopold, L., Wolman, M. and Miller, J. 1964. Fluvial processes in geomorphology. Freeman, San Francisco. 522 pp.

Leopold, L. and Wolman M. 1957. River channel patterns- braided, meandering and straight. Report No.: 282-B.

Leopold, L. 1994. A view of the River. Cambridge, MA: Harvard University Press. 298 pp.

MacCarter, L., Fields, J., Smith, D. 2016. Large Woody Debris on the Carmel River from Camp Steffani to the Carmel Lagoon, Fall 2015: Watershed Institute, California State University Monterey Bay, Publication No. WI-2016-05, 25 pp.

[MEI] Mussetter Engineering, Inc., 2003. San Clemente Reservoir and Carmel River Sedimenttransport Modeling to Evaluate Potential Impacts of Dam Retrofit Options. Prepared for American Water Works Service Company, Voohees, NJ, April, 304 p.

[MEI] Mussetter Engineering, Inc., 2005. Hydraulic and Sediment-transport Analysis of Carmel River Bypass Option, California. Prepared for California American Water. April 25.

Nicol, C. Smith, D., Watson, F. 2014. Exploring particle density effects on partial entrainment of steelhead spawning gravels: River Research and Applications. DOI: 10.1002/rra.2726.

Ritter, D., Kochel, R., Miller, J. 2011. Process geomorphology (5th edition). Waveland Press Inc., Long Grove. 652 pp.

Rosenberg, L. 2001, Geologic Resources and Constraints, Monterey County, California: A Technical Report for the Monterey County 21st Century General Plan Update Program, prepared for County of Monterey Environmental Resource Policy Department, 91 pp.

Rosgen, D. 1994. A Classification of Natural Rivers. Catena, 22, 169-199.

Rosgen, D. 1996. Applied River Morphology. Pagosa Springs, CO. Wildland Hydrology.

Rosgen, D. 2006. Watershed Assessment of River Stability and Sediment Supply (WARSSS) (2nd edition 2009). Fort Collins, CO. Wildland Hydrology.

Schumm, S. 2005. River Variability and Complexity. Cambridge University Press. 220 pp.

[SDR] San Clemente Dam Removal and Carmel River Reroute Project Website. http://www.sanclementedamremoval.org/. Last accessed: May 19, 2016.

Smith, D., Newman, W., Watson, F. and Hameister, J. 2004, Physical and Hydrologic Assessment of the Carmel River Watershed, California. The Watershed Institute, California State University Monterey Bay, Publication No. WI-2004-05. 83 pp.

Smith, D., Diehl, T., Turrini-Smith, L., Maas-Baldwin, J, and Croyle, Z. 2009, River restoration strategies within channelized, low-gradient landscapes of West Tennessee, USA; in James, A., Rathburn, S., and Whittecar, R., eds, Management and Restoration of Fluvial Systems with Broad Historical Changes and Human Impacts: GSA Special Paper no 451, p. 215-229.

URS 2012. Project number 26818107. Project base map. http://www.sanclementedamremoval.org/wp-content/uploads/2011/08/CRRDR-Proposed-Project.jpg. Last accessed: May 19, 2016.

[USGS] USGS 11143200 Carmel R A Robles Del Rio Ca. [Internet]: United States Geological Survey; [cited 2016]. Available from: http://waterdata.usgs.gov/nwis/inventory?agency_code=USGS&site_no=11143200.

Ward A., Trimble S., Burckhard S. and Lyon J. 2016. Environmental Hydrology. 3rd ed. NW: CRC Press. 663 pp.

White, F. (1976). Fluid Mechanics (2nd edition). McGraw Hill Book Company, San Francisco. 732 pp.

Wolman, M., and Miller, J. 1960. Magnitude and frequency of forces in geomorphic processes. J. Geol. (68): 54-74.

8 Appendix A

Visual Assessment Key

BANK STABILITY	**Criteria** **Bank Condition**	**Location**	**Condition (1-3)** 1-significantly eroded 2- damaged 3-good			
	FES		**Condition (1-3)** 1-removed 2- damaged 3-good	**Herb vs Wood (1-3)** 1-most herb. 2-equal parts 3- most wood	**Veg. Transition (1-3)** 1-FES 2-equal parts 3- full trans.	**Veg Symmetry(0/1)** 0-no 1-yes
	Floodplain		**New Deposits (0/1/2)** 0-none 1-some 2- a lot	**Herb vs Wood (1-3)** 1-most herb. 2-equal parts 3- most wood	**Seed Boulder Movement (0/1)** 0-no 1-yes	**LWD (0/1)** 0-absent 1-present (quantity)
CHANNEL	**Channel**		**Lateral Failure (0/1/2)** 0-none 1-incipient 2-full	**Vert. Failure (0/1/2)** 0-none 1-incipient 2-full	**Cobbly Corner Fill (1-3)** 1-missing 2- damaged 3-good	**Structural Adj. (0/1/2)** 0-none 1-some 2- a lot
			Step Pool Infilling (0/1) 0-no 1-yes	**Fish or Frogs (0/1)** 0-no 1-yes		
	LWD-recruited		**Presence (0/1)** 0-absent 1-present (quantity)	**Structure (0/1)** 0- passive 1- yes (bed/bank)	**Scouring (0/1)** 0- passive 1- yes (bed/bank)	
	LWD-structural		**Condition (1-3)** 1-missing 2-adjusted 3-good	**Recruiting (0/1)** 0-no 1-yes		

9 Appendix B

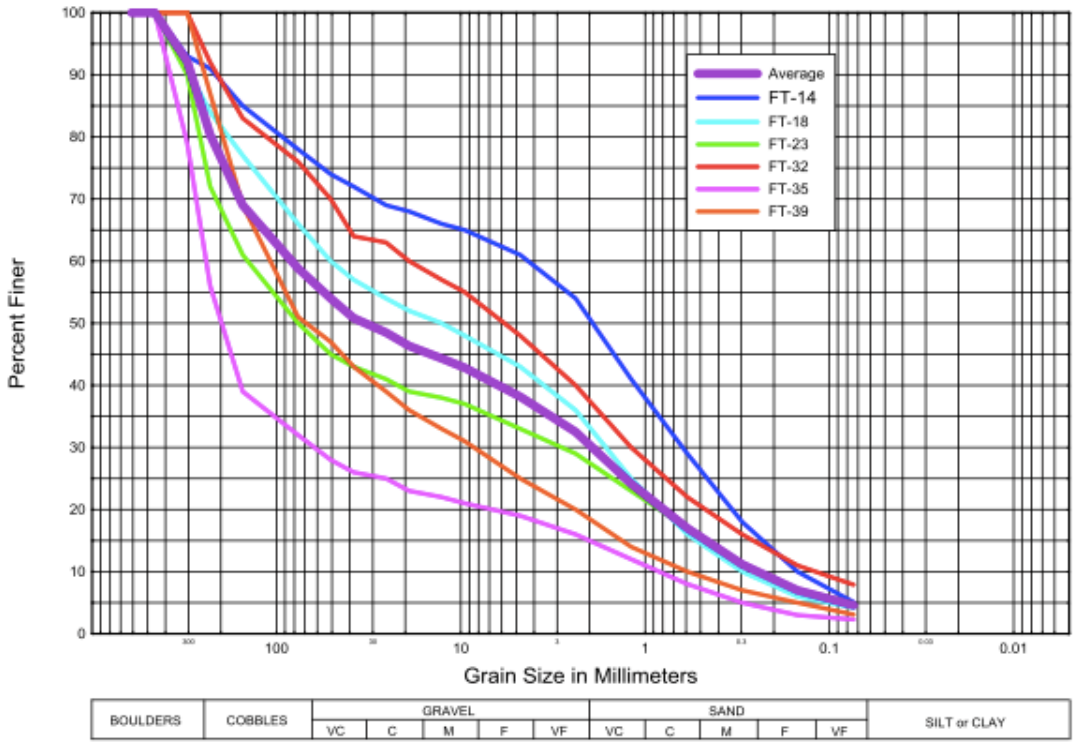

Particle size gradation curves from the in-channel pits (Tetra Tech 2015)

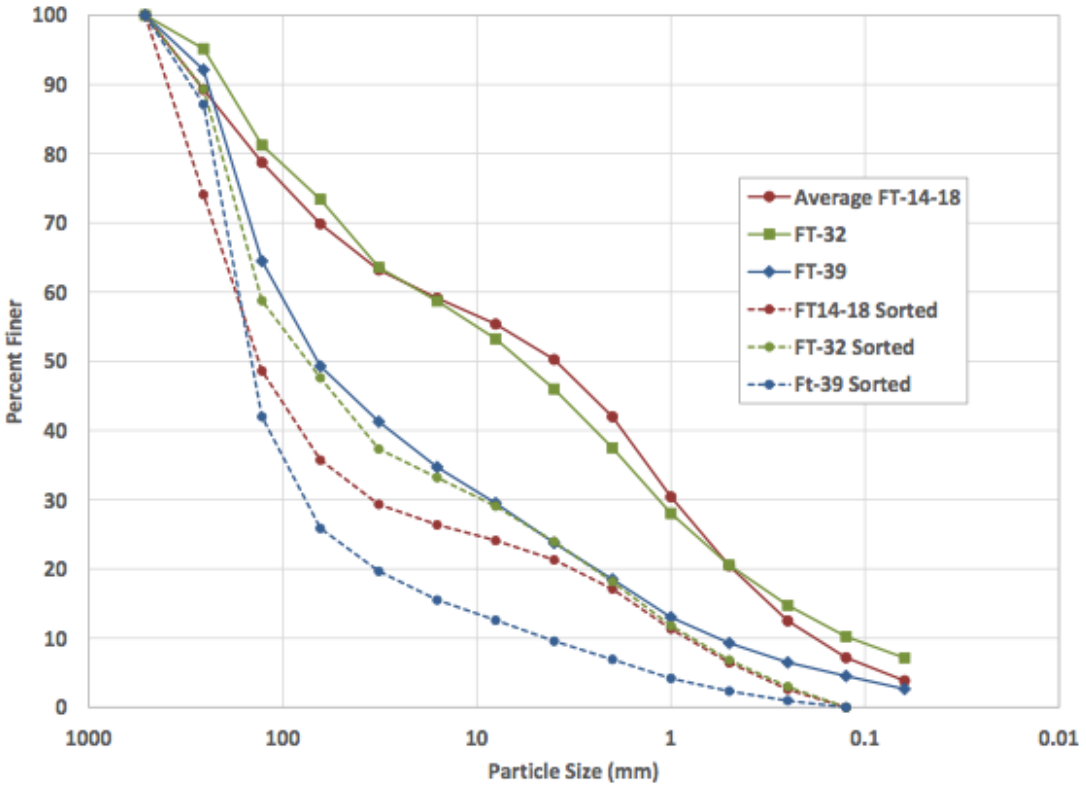

Gradation from sieve analysis of material from Test Pits FT-14, FT-18, FT-32 and FT-39. Also graphed are the estimated surface gradations that would develop as the material adjusts during a 5-year flow (Tetra Tech 2015).